NIRS

HIMAC

NIRS-M-91
HIMAC-004

# Irradiation of 135 MeV/u carbon and neon beams for studies of radiation biology

T.Kanai, S.Minohara, T.Kohno, M.Sudou, E.Takada,
F.Soga, K.Kawachi, A.Fukumura and F.Yatagai

March 1993

National Institute of Radiological Sciences

9-1, Anagawa 4-chome, Inage-ku, Chiba-shi 263 JAPAN

# Irradiation of 135 MeV/u carbon and neon beams for studies of radiation biology

Tatsuaki Kanai[1)], Shinichi Minohara[1)], Toshiyuki Kohno[1)], Michio Sudou[1)], Eiichi Takada[1)], Fuminori Soga[1)], Kiyomitsu Kawachi[1)], Akifumi Fukumura[2)] and Fumio Yatagai[3)].

[1)]Division of Accelerator Research,
[2)]Division of Physics,
National Institute of Radiological Sciences
[3)]Cellular Physiology Laboratory,
RIKEN ( The Institute of Physical Chemical Research )

*ABSTRACT*

*A heavy ion irradiation system was designed and constructed at RIKEN ring cyclotron facility for studies of radiation physics and radiation biology. Carbon and neon beams of 135 MeV/u were firstly used for the experiments. A pair of wobbler magnets and a scatterer were used for obtaining the uniform radiation field of about 10 cm in diameter. A parallel plate ionization chamber was used for dose monitoring. A range shifter was used for degrading the initial energy of the heavy ions. Precise depth dose distributions were measured by a small parallel plate ionization chamber and a variable length water column. LET(linear energy transfer) of the heavy ion radiation fields were measured by a parallel plate proportional chamber. From these basic measurements, biological experiments using these heavy ions are now carried out at this facility.*

## INTRODUCTION

Biological researches with heavy ions have been studied over 30 years since the works by Barendsen[1]. It has been proved that investigations using heavy ions are very important to understand a mechanism of radiation effects on biological species[2]. Although many properties of the heavy ions on biological species have been studied, there are problems to be solved yet, such as dependence of RBE(relative biological effectiveness), OER(oxygen enhancement ratio), or repair capacity etc. upon LET( linear energy transfer). With the heavy ion beams, it is relatively easy to modulate the beam and to make desired LET distributions. This is the most important aspect of the heavy ion beam.

Because of their good dose localization and high biological effectiveness, the heavy

ion beams are expected to improve clinical results of radiation therapies. Clinical trials have been performed at LBL ( Lawrence Berkeley Laboratory, University of California) using Bevalac[3]. Also at NIRS (National Institute of Radiological Sciences in JAPAN), HIMAC (Heavy Ion Medical Accelerator in Chiba) facility for the heavy ion radiation therapy is now under construction[4]. Clinical trials at NIRS are scheduled to start in 1994. In addition it becomes very important to investigate biological effects of galactic ray or cosmic ray for space sciences. High Z particles, such as Fe, in the galactic ray are expected to have much influence on biological species[5].

The RIKEN ring cyclotron offers very suitable heavy ion beams for the above investigations[6]. At the ring cyclotron, heavy ions, whose atomic number is less than 10, can be accelerated to the energy of 135 MeV/u and heavier ions up to Xe can also be accelerated. A facility which irradiates the heavier ions for small fields was already installed at the ring cyclotron facility[7]. But it was necessary to construct another irradiation facility which realized a large radiation field of around 10 cm in diameter and is suitable for biological experiments using heavy ions of $Z \leq 10$. Therefore, a new irradiation system has been constructed at the RIKEN ring cyclotron facility for the irradiation of these heavy ion beams. Pioneering works of radiation biology with high energy heavy ion beams have been performed at LBL(Lawrence Berkeley Laboratory, California in U.S.A.) and GSI(Gesellschaft fur Schwerionenforschung, Darmstadt in Germany) since 1970s and 1990, respectively. LBL firstly used an occluding ring[8] and then changed the system to a wobbler system[9] to make uniform irradiation fields for the heavy ion radiation therapy. Biological experiments have been performed using the same system as the therapy course at LBL. GSI adopted a raster scanning method to make the radiation field[10].

In this paper, detail of the beam course installed at RIKEN ring cyclotron facility is presented and physical characteristics of the carbon and neon ion beams are described.

## IRRADIATION FACILITY

Figure 1 shows an illustration of an irradiation system for biological experiments installed at the irradiation room E5 in the RIKEN ring cyclotron facility. The irradiation system comprises wobbler magnets, a scatterer, a beam monitor, a range shifter, a range modulator, a collimator and a sample changer. In order to make a uniform irradiation field, we used a pair of wobbler magnets and the scatterer[9,11]. The range shifter is used for changing LET (Linear Energy Transfer) at the irradiation site. The range modulator is used for making a spread-out Bragg peak.

*Uniform irradiation field*

During the exposure in the biological and physical experiments, the accelerator extraction system is usually tuned a little in order to keep beam intensity constant. Because of this fine tuning, the shape and the position of the transported beam at the

irradiation site are expected to change. In order to minimize the influence of these fluctuations of beam characteristics on the uniformity of the irradiation field, the beam was focused on the irradiation site by the beam delivering system. During the initial tuning of the transport system, a zine phosphor sheet was set at the irradiation site and the image of the beam spot gleaming on the sheet was monitored by a TV camera. The size of the focused beam was usually around 5 mm in diameter.

The wobbler magnets were duplicated from the magnets installed at the beam course for heavier ions[7]. Specifications of the wobbler magnets are described in Table 1. A magnetic rigidity for 135 MeV/u carbon beam is 3.465 Tm. Distances from the magnets to the irradiation site are 6.445 and 5.995 m. Sine and cosine wave currents are supplied to the magnets. The focused beam can draw a circular shape at the irradiation site with these wobbler magnets. A maximum radius of the circular trace of the 135 MeV/u carbon beam is 6.6 cm at the irradiation site. Figure 2 shows the distance off the central beam axis of the wobbled beam versus remote control voltage to the power supply, which is proportional to the current of the wobbler magnets. The distance was obtained by measuring the radius of the trace of the beam lightened on the zine phosphor screen. The linear relationship between the beam radius and the remote control voltage held for the radii from 15 mm to 60 mm. Figure 3 shows a typical picture of the circular trace of the wobbled beam gleaming on the zine phosphor screen.

In order to make a uniform flat field, the wobbleded beam was scattered. A gold scatterer was used for the beam broadening because ions were scattered by high Z materials much more efficiently than by low Z materials for the same energy loss in the scatterer. A gaussian angular distribution of the incident beam intensity was realized by the multiple scattering in the scatterer. Open circles in Fig. 4 show a intensity distribution of 135 MeV/u carbon beam at the irradiation site scattered by the gold scatterer of 0.27 mm thickness. A solid curve in the figure shows a gaussian function fitted to the measured data. The data were measured by scanning a small ionization chamber at the irradiation site, whose sensitive area is 5 mm in diameter. The chamber was used for the measurements of the lateral dose distributions and also for measurements of depth dose distributions in our experiments. Figure 5 shows root mean squares of the scattered angles for 95 MeV/u Ar, 135 MeV/u C and 135 MeV/u Ne beams by gold scatterers. The root mean squares of the scattering angles were derived by radii where the intensity went down to 1/e of the maximum intensity of the gaussian distribution divided by the distance between the scatterer and the irradiation site. Solid and dashed curves were results of the multiple scattering angle for 95 MeV/u Ar and 135 MeV/u C beams calculated by Moliere theory[11]. Open triangle, open circle and closed circle in Fig. 5 indicate the measured scattering angle of 95 MeV/u Ar beam by a 0.17 mm gold scatterer, of 135 MeV/u C and Ne beam by a 0.27 mm gold scatterer, respectively. The multiple scattering angles for 135 MeV/u C and Ne beams were almost equal each other. The measured and the calculated scattering angles agreed very well as shown in Fig. 5.

By wobbling the scattered beam with a radius of 56.7 mm, a uniform irradiation field was realized as a solid curve shown in Fig. 6[8,9]. In this method, the beam intensity

of the central part of the irradiation field will decrease when the wobbling radius becomes larger. A dashed curve in Fig. 6 indicates the intensity distribution obtained by the wobbling radius of 60 mm. We determined the wobbling radius of the incident beam so that the difference between the intensity at the central part and that at the peripheral highest part is less than 2.0 % of the average intensity of the irradiation field. At this condition, the uniform irradiation field of around 10 cm in diameter was realized as shown in Fig. 6.

*Irradiation beam monitor*

The wobbled and scattered beam was extracted from a vacuum pipe through a 50 μm aluminum sheet. At just downstream of the vacuum window, a parallel plate ionization chamber was placed as an irradiation dose monitor. Figure 7 shows an illustration of the irradiation dose monitor. Aluminum sheets of 15 μm thick were used for signal and high voltage electrodes. The signal electrode was sandwiched by the high voltage electrodes with gaps of 10 mm. The chamber was filled with air. Formula of the current suppression by a general recombination is well established for a parallel plate ionization chamber in the field of high energy electron or photon beams. If it is also valid for the heavy ion radiation field, the effect of the general recombination is less than 0.5 % at usual dose rate of around 5 Gy/min when 1500 V is applied to the high voltage electrode[12]. The output current of the monitor was fed into a current-to-frequency converter(I-F converter), which made a pulse per 100 pC of the output charge of the chamber monitor(see Fig. 10). Maximum pulse rate of the I-F converter was about 500 kHz.

*Range shifter*

A range shifter was placed between the irradiation site and the dose monitoring ionization chamber. The range shifter consisted of two large wheels, and 8 absorber sheets were mounted on each wheel. The combination of the two absorbers in each wheel realized 64 kinds of absorber thicknesses. This range shifter was used for degrading the beam energy. Radiation fields of various LET values can be realized by choosing an appropriate absorber thickness. Depth dose distributions were also obtained by measuring ionization currents of the small ionization chamber placed at the irradiation site for various absorber thicknesses of the range shifter. In order to measure the Bragg curves efficiently, the ionizations were measured in small intervals near the Bragg peak and in rough intervals around the entrance positions. For the specified heavy ion beams, we prepared specific sets of the range shifter absorbers.

*Range modulator*

A range modulator was installed beside the range shifter for making a spread-out Bragg peak. For a radiation therapy, it is very important to develop a method for designing the range modulator. In order to decrease irradiation dose to normal tissue, we have to make a spread-out Bragg peak in which the biological response is uniform over

the region of interest. We have made two kinds of range modulators to investigate how to design the spread-out Bragg peak for radiation therapy. One was designed so as to have the flat biological response in the spread Bragg peak. And the other was designed so as to have a flat physical dose distribution in the spread Bragg peak to irradiate massive biological objects.

*Other devices*

At the irradiation site, a final beam collimator and a sample changer were installed. For measuring the beam intensity distributions in Figs. 4 and 6, the small ionization chamber was scanned by the sample changer. For irradiating the biological objects sequentially, many samples also can be set on the sample changer and the aperture of the collimator is adjusted according to the size of the samples. A water column was usually used at the irradiation site in the measurements of depth dose distributions in water. Figure 8 shows pictures of the irradiation course.

*Control System*

Figure 9 shows a block diagram of the control system for the beam irradiation system. The devices were controlled by a microcomputer PC9801 RX (NEC Co.) through GPIB interface. The scintillator in the figure was used for a fluence measurement in the dosimetry of the heavy ion irradiation field[13]. The LET, the ΔE-E counters were used for LET measurements and particle identification measurements, respectively. The ionization chamber was used for measurements of lateral dose distributions of the irradiation fields together with the sample changer to change the position of the chamber. This chamber was also used for measurements of depth dose distributions together with the water column or the range shifter. The output of the I-F converter of the monitor was fed to the fast counter. The fast counter had an output signal, whose level was high during the counting. The output signal was used to control the beam shutter. Then the beam shutter was open while the counter was working. The pulse train from the I-F converter was also fed to the rate meter, which was used for monitoring the beam intensity during the irradiation.

Figure 10 shows a flow chart of the program "PROFILE" which controls the sample changer, the electrometer and the fast counter in order to measure the beam profile by the small ionization chamber. First, a preset count, which determines irradiation dose of each position, is set on the fast counter. Scanning positions, where dose is to be measured, are read. Then, the detector moves to the first position by the pulse motor controller of the sample changer. After the detector stppes, the procedure of the charge measurements by the electrometer is started. The fast counter starts to count the output pulse train from the I-F converter of the beam monitor. The beam shutter is open while the counter is working. When the counter is stopped with the preset count, the beam shutter is closed. The charge measured by the electrometer is read and stored into the computer memory. The procedure of the charge measurement finishes with resetting the electrometer. Then the detector moves to the next position and the charge measurement

by the electrometer is repeated.

Figure 11 shows the flow chart of the program "BRAGG" which controls the range shifter, the water column, the electrometer and the fast counter to measure Bragg curves. First, the preset count is set on the fast counter. The absorbers of the range shifter are chosen and the thickness of the water column is set through the pulse motor controllers. Next the program goes to the charge measurement routine as the same as the "PROFILE" program. After finishing a charge measurement, the program repeats the charge measurement again, or goes back to the preset counter routine, or the range shifter setting routine, or the water column setting routine.

Figure 12 shows the flow chart of the program "EXPOSURE" which controls the range shifter, the fast counter and the sample changer to expose samples. First, the absorber number, the distance between neighboring samples, the calibration constant of the dose monitor (Gy/count), and the irradiation doses are input. Then the first sample is set at the center of the irradiation field. And the preset count, which is obtained from the irradiation dose and the calibration constant, is set on the fast counter. Next, the fast counter is started. Then the beam shutter is open until the counter reaches to the preset count. After finishing the irradiation, the next sample is set at the center of the irradiation field. And the exposure is repeated.

Once the whole procedures are set in these programs, all subsequent steps are proceeded automatically and the measurements are performed with high efficiency.

## DEPTH DOSE DISTRIBUTION

Dosimetry for the irradiation of the heavy ion was described in a separate paper[13]. Fluence of the uniform irradiation field was measured by a plastic scintillator, and dose at the entrance position of the depth dose distribution was obtained by multiplication of the fluence by the stopping power of the heavy ions at the position.

Depth dose distributions were measured by the small ionization chamber. The chamber was a parallel plate ionization chamber and had an entrance window of 2.5 μm aluminized polyester sheet, which played also as a high voltage electrode. A signal electrode was 5 mm in diameter surrounded by a guard ring. The gap between the signal and the high voltage electrodes was 2 mm. Air was used for the chamber gas.

The depth dose distributions were measured by changing the absorber thickness of the range shifter or by changing thickness of the water column. The absorber thicknesses of the range shifter were chosen so as to get the Bragg peak in the depth dose distribution of the monoenergetic heavy ion beam. The water equivalent thickness of each absorber in the range shifter was deduced from the positions of two Bragg peaks, which were obtained by changing thickness of the water column, with and without the absorber. The difference between the depth of the two Bragg peaks corresponds to the water equivalent thickness of the absorber. In Table 2, the thicknesses of the absorbers of the range shifter are listed for the cases of 135 MeV/u carbon and neon beams, respectively. In order to get adequate data points around the Bragg peak, thicknesses of the absorbers

mounted on the first wheel of the range shifter were chosen in around 350 μm step. Thicknesses of the absorbers mounted on the second wheel for the case of neon beam were around half of those for the case of carbon beam because the range of the neon beam is 2 cm, which is about half of the range of the carbon beam.

Detailed depth dose distributions in water were obtained by changing thickness of the water column, which was placed at the irradiation site. The water column had an entrance and an exit window of 1 mm Lucite. Although the thickness of the water column can be set in 10 μm accuracy relative to a point of origin, the absolute thickness of the water column at the origin should be measured by other means. In order to get the water equivalent thickness of the origin of the water column, the two Bragg curves obtained by the range shifter and the water column were compared. Horizontal axes of the two Bragg curves were corresponding to the thickness of the water absorber. When the Bragg curve of the water column is horizontally shifted and multiplied some factor in order to overlap completely with the Bragg curve of the range shifter, the shift length corresponds to the water equivalent thickness of the origin of the water column. The shift length was obtained by least square fit of the Bragg curve and the shifted Bragg curve obtained by the range shifter and by the water column, respectively. Figure 13 shows the comparison of the two Bragg curves in the case of 135 MeV/u carbon beam. Open circles and closed triangles are showing the shifted Bragg curve measured using the water column and the Bragg curve measured using the range shifter, respectively. The shift length was 5.059 mm in that case. The shape of the Bragg curve agreed completely each other. Although the distance between the range shifter and the irradiation site was around 20 cm, Bragg curve distortion due to the multiple scattering in the range shifter was negligible.

This depth dose distributions should be modified by effects of an energy dependence of differential W value (w), difference of the w value for primary particle and secondaries, and the initial recombination in the measurement of the ionization charge. Since there are a few data concerning to the w value, we assumed the constant w value at present.

*Initial Recombination*

The depth dose distributions were measured with the small ionization chamber with high voltage of 400 V. As discussed in reference [11], an initial recombination plays an important role in measuring the ionization current of an air-filled parallel plate ionization chamber. The parallel plate ionization chamber is the best ionization chamber for measuring the depth dose distribution of heavy ion beams, because the depth of the measuring point can be well determined when the parallel plate is put perpendicular to the beam axis. When a thimble chamber is used for the dosimetry, the pathlengths from absorber surface to the central and edge part of the chamber are different each other. Then the sharp Bragg peak may be broadened by this effect. In Fig. 14, inverses of the ionizing current were plotted against inverses of the applied high voltage at the various depth in water for 135 MeV/u neon beam. The inverses of the ionization currents in the

figure were normalized by that at the high voltage of 400 V. The data corresponding to $1/V < 0.01$ can be fitted by a straight line. As shown in the figure, the slopes of the plot were steeper as the values of LET were larger. The extrapolated values at the infinite voltage, what is $1/V=0$, indicate the real ionization currents. Figure 15 shows the LET dependence of the slope for carbon and neon beams. As shown in Fig. 15, the slope increased almost linearly as the value of LET increased except near the Bragg peak. Near the Bragg peak, the beam is not monoenergetic and has a wide LET distribution. Perhaps, the slope of the recombination curve for the case of the broad LET spectrum is not a function of the dose average LET. Figure 16 shows the LET dependence of the extrapolated values. The depth dose curves can be corrected by this figure. Figures 17 and 18 show the depth ionization curves for 135 MeV/u carbon and neon beams, respectively. Open circles in the figures are the raw data of the ionization currents and solid curves are the ionization currents corrected by the initial recombination. The distortion of the depth dose distributions due to the initial recombination was not so large as shown in the figures.

## LET MEASUREMENTS

Linear energy transfer ( LET ) is the most important physical quantity when we discuss the biological response to heavy ion beams. In case of low energy ion beams, LET is obtained by calculation very accurately. In case of high energy heavy ion beams, on the contrary, it is very difficult to calculate the LET because of contributions from fragmented nuclei. Then, we measured the LET by a parallel plate proportional counter. The counter had two anode wires, whose spacing was 5 mm. The anode wires of 30 μm in diameter were sandwiched between the parallel plate cathodes. The gap between the anode and the cathodes was 2.5 mm. We used 2.5 μm aluminized polyester film as the entrance window of the counter. Tissue equivalent gas ( $C_3H_8$ 54.6%, $CO_2$ 40.14%, $N_2$ 5.26% by volume) was flowed through the counter during the measurements. An annular shaped plastic scintillator was placed in front of the LET counter. Diameter of the hole of the plastic scintillator was 5 mm. The signal from the scintillator was used as an anti-coincidence gate to the LET counter. Then, signals of the heavy ions which pass through the central part of the counter were analyzed by a pulse height analyzer system. Tissue equivalent gas of 5 mm thick at 760 torr is corresponding to 5 μm thick of the tissue material with density 1. Details of the particle identification system will be discussed elsewhere.

## RESULTS AND DISCUSSIONS

Figure 19 shows a depth dose distribution in water for 135 MeV/u carbon beam. Open circles in the figure show experimental results measured by the ionization chamber. The experimental data were corrected according to the LET dependence of the initial recombination. Solid curve is a theoretical result. For the primary beam, the calculation

took account of the effects of a range straggling and a fluence reduction due to nuclear reactions of the incident particles with target nuclei. The calculation also took account of a fragmentation effect, that is to say, dose contributions of secondary and tertiary nuclei produced by nuclear reactions[14,15]. In the calculation, the fragmented nucleus was assumed to have the same velocity as the primary particle when the nucleus was produced. A few percents of the entrance dose were deposited in the region deeper than the Bragg peak. The dose in this region is contributed by the fragmented nuclei. Then we call this dose contribution as "fragmentation tail". Because the energy of the incident beam was relatively low, the dose contribution by the fragmented nuclei was less than 10 % of the entrance dose. As shown in Fig. 19, the experimental data agree with the theoretical result very well except for the data very near the Bragg peak. Figure 20 shows the expanded dose distribution near the Bragg peak. The peak height of the experimental result was lower than that of the theoretical result. This discrepancy can be caused by the following two reasons. One is the momentum spread of the beam, which was neglected in the calculation. The other is the energy dependence of the differential W value of the heavy ions. If the incident beam has the momentum spread, the height of the Bragg peak becomes lower and the width of the Bragg peak becomes wider than those of the original Bragg peak. The theoretical Bragg peak width was wider than the experimental width as shown in Fig. 20. If the differential W value becomes larger as the energy of the heavy ion becomes lower, the height of the Bragg peak of the experimental result becomes lower and the width becomes wider than those of the theoretical result. Figures 21 and 22 show the depth dose distribution in water for 135 MeV/u neon beam and its expanded distribution, respectively. Open circles in the figures are the experimental results, which were corrected by the initial recombination effect, and the solid curve is the result of theoretical calculation. The height of the Bragg peak of the experimental result was again lower than that of the theoretical one. But the width of the Bragg peak was the same each other. Then, the discrepancy may be explained by both of the two reasons, the momentum spread of the incident beam and the energy dependence of the differential W value.

Figures 23 and 25 show the dose average LET for 135 MeV/u carbon and neon beams, respectively. Figures 24 and 26 are the expanded figures of the Figs. 23 and 25, respectively. Open circles in the figures are the experimental results and the solid curves are the theoretical results. The theoretical results agreed with the experimental values except again near the Bragg peak, especially in the carbon case.

*Dose Calibration Procedure*

When the depth dose distribution is measured and the absolute dose at the entrance position is measured by the fluence measurement method, dose per monitor count can be determined. Because of daily fluctuation of the extracted energy of the heavy ions, we usually measure Bragg curve using the range shifter for the dose calibration. Figure 27 shows the procedure of the dose calibration with the result of the Bragg curve measurement. First the data of the Bragg curve using the range shifter and the reference

data which include the depth, dose and LET are read from the hard disk. The distance between the two Bragg peaks is calculated. Then the LET (stopping power of the heavy ion in water) are interpolated from the reference data. The absolute dose at the entrance position is calculated by multiplying the LET by the measured fluence. We can also deduce the absolute dose with the differential W value obtained by a comparison of the fluence dosimetry and the ionization chamber dosimetry. Assuming the differential W value is constant, we determine the dose for the deeper region by multiplying the absolute dose at the entrance position and the relative ionization value. Except very near the Bragg peak, the described dosimetry is good enough for the biological experiments.

## Conclusion

The irradiation field realized by this facility is around 10 cm in diameter. And the uniformity in beam profile was very good. Then, many biological systems, such as cultured cells, spheroid, small fishes, mice and so on, can be irradiated at various LET with the carbon and neon beams. Using this irradiation and dosimetry system, many biological experiments are now performed at the RIKEN ring cyclotron facility[16].

### *Acknowledgments*

*We would like to express sincere gratitude to the Institute of Physics and Chemistry Research (RIKEN), who provided us an opportunity to construct an irradiation port and to do heavy ion experiments using the Riken ring cyclotron (RRC). We are very grateful to the crew at RRC for delivering excellent beam during the experiments.*

## REFERENCES


[1] G.W.Barendsen and T.L.J.Beusker, Effects of different ionizing radiations on human cells in tissue culture. II Biological experiments. Radiat. Res. 13, 841–849 (1962).

[2] LBL report, " Biological and Medical Research with Accelerated Heavy Ions at the Bevalac, 1977–1980.",C.Pirrucello and C.A.Tobias, Editors, LBL report Univ. Calif. LBL–11220.

[3] J.R.Castro and M.M.Reimers, Charged particle radiotherapy of selected tumors in the head and neck. Int. J. Radiation Oncology Biol. Phys. 14, 711–720 (1988).

[4] Y.Hirao et al., Heavy ion medical accelerator in Chiba. – A design summary and update –. HIMAC report, HIMAC–001 (NIRS–M–89) 1992.

[5] W.Schimmerling, Radiobiological problems in space, An overview. Radiat. Environ. Biophys. 31, 197–203 (1992).

[6] Y.Yano, Status Report on Riken Accelerator Research Facility. The 8th Symp. on Accelerator Science and Technology, 1991, Saitama, Japan. 10–12, (1991).

[7] T.Takahashi, private communication.

[8] T.R.Renner and W.T.Chu, Wobbler facility for biomedical experiments. Medical Physics 14, 825–834 (1987).

[9] T.Kanai, K.Kawachi and T.Hiraoka, An irradiation facility and a beam simulation program for proton radiation therapy. Nucl. Instru. Methods, A302, 158–164, (1991).

[10] GSI Biophysics group, Design, construction and first experiments of a magnetic scanning system for therapy. GSI–91–18 report, (1991).

[11] V.G.Moliere, Theorie der Streuung schneller geladener Teilchen II, Mehrfach– und Vielfachstreuung. Z.Naturforschg. 3A, 78–97 (1948).

[12] J.W.Boag, Ionization chambers, in "Radiation Dosimetry vol. II", edited by F.H.Attix and W.C.Roesch, Academic Press, New York and London, 1966.

[13] T.Kanai et al., Dosimetry and measured differential W values of air for heavy ions. submitted to Radiation Research.

[14] L.Sihver and T.Kanai, Energy loss, range and fluence distributions, total reaction and projectile fragmentation cross sections in proton–nucleus and nucleus–nucleus interactions. HIMAC report, NIRS–M–87 (HIMAC–002), July 1992.

[15] T.Kanai and L.Sihver, to be published.

[16] Proceedings of the second workshop on physical and biological research with heavy ions. (Edited by K.Ando and T.Kanai), HIMAC report, NIRS–M–90 (HIMAC–003), Aug. 1992.

Table 1 Specification of wobbler magnets

| | |
|---|---|
| Pole gap size (mm) | 60 |
| Pole length (mm) | 300 |
| Maximum magnetic field (T) | 0.127 |
| Maximum current (A) | 20 |
| Number of turns | 318 x 2 |
| Inductance (H) | 0.11 |
| Frequency (Hz) | 60 |

Table 2. Absorber thickness of the range shifter.

| No | 135MeV/u C (mm) | 135MeV/u Ne (mm) |
|---|---|---|
| 1 | 0.35 | 0.35 |
| 2 | 0.59 | 0.59 |
| 3 | 0.95 | 0.95 |
| 4 | 1.27 | 1.27 |
| 5 | 1.59 | 1.59 |
| 6 | 1.90 | 1.90 |
| 7 | 2.25 | 2.25 |
| 8 | 11.42 | 3.84 |
| 16 | 23.10 | 8.15 |
| 24 | 28.97 | 11.42 |
| 32 | 34.974 | 14.98 |
| 40 | 37.284 | 19.53 |
| 48 | 39.618 | 21.929 |
| 56 | 42.021 | 23.10 |

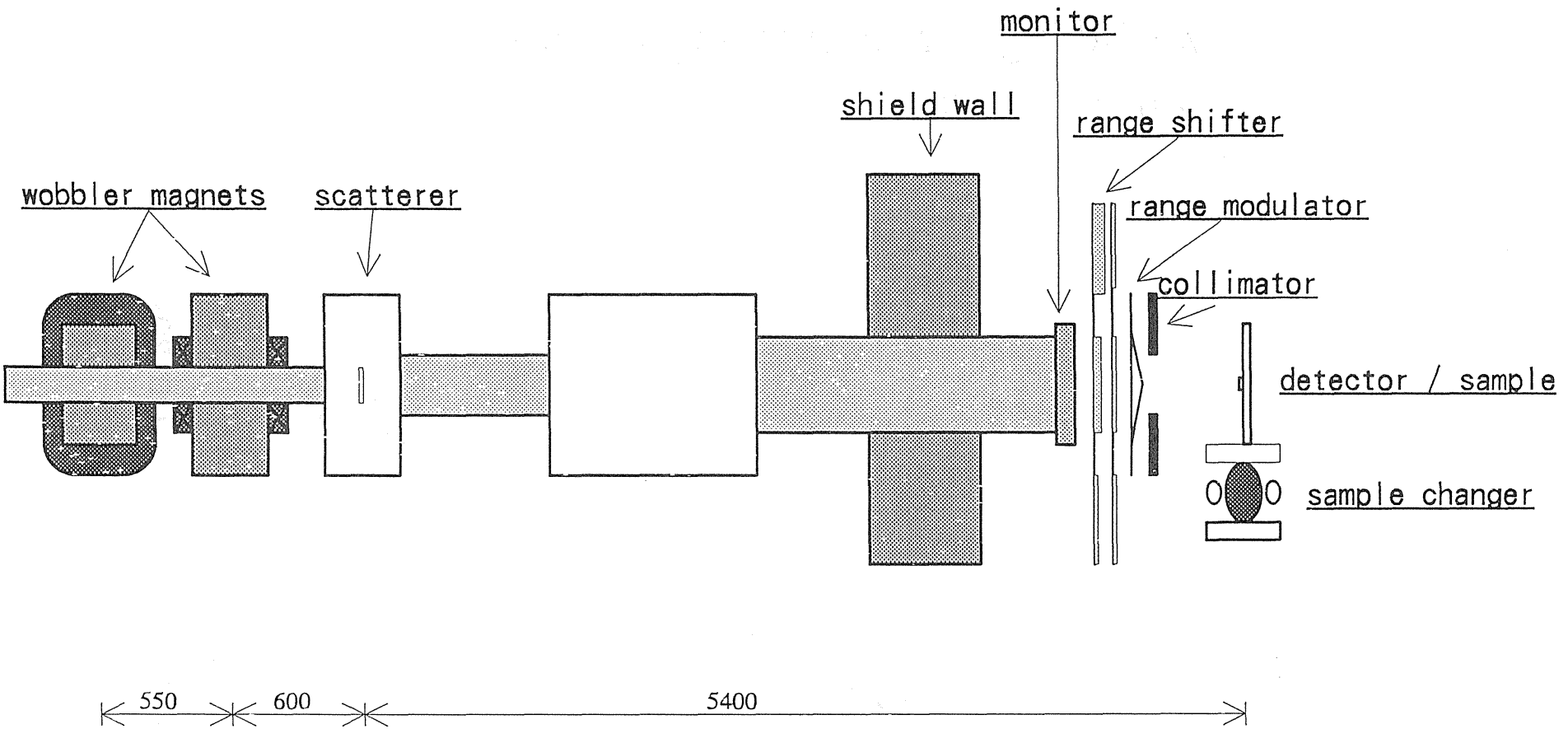


Fig. 1. Schematic layout of the irradiation system installed at the RIKEN ring cyclotron facility.

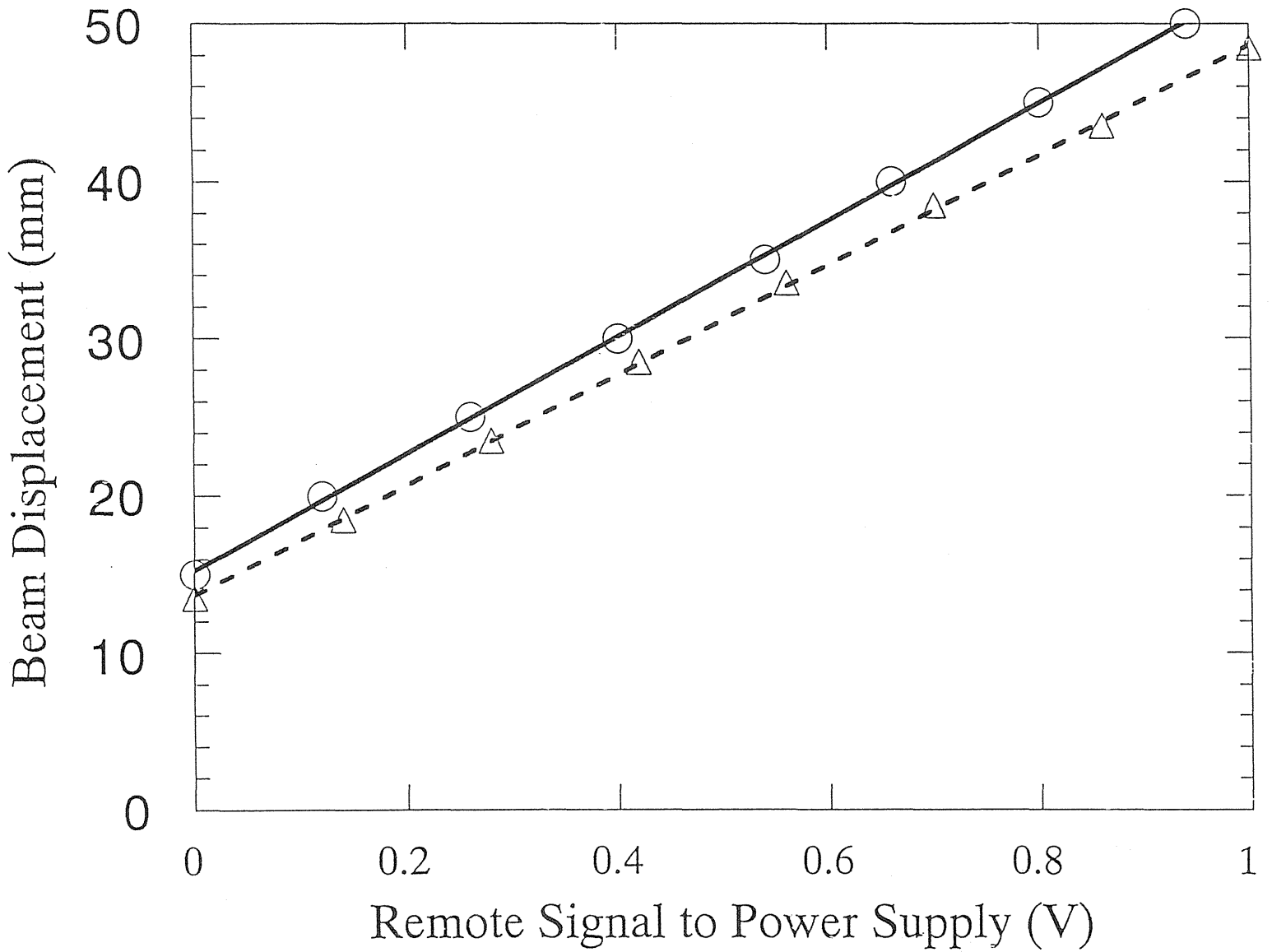


Fig. 2. Displacements of the carbon beam versus remote control voltages to the power supplies of X and Y wobbler magnets.

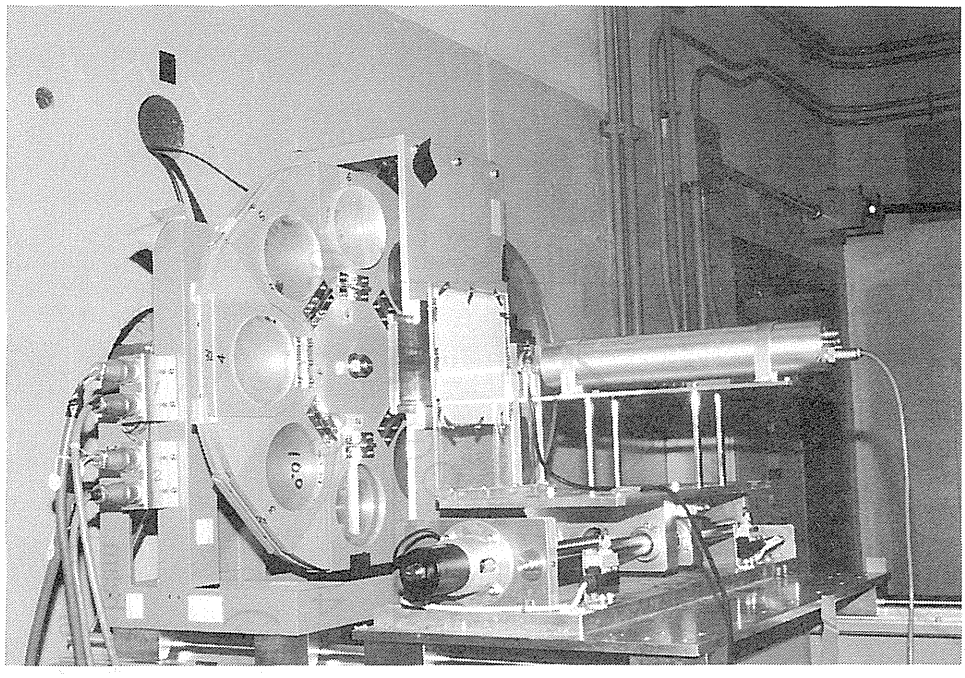

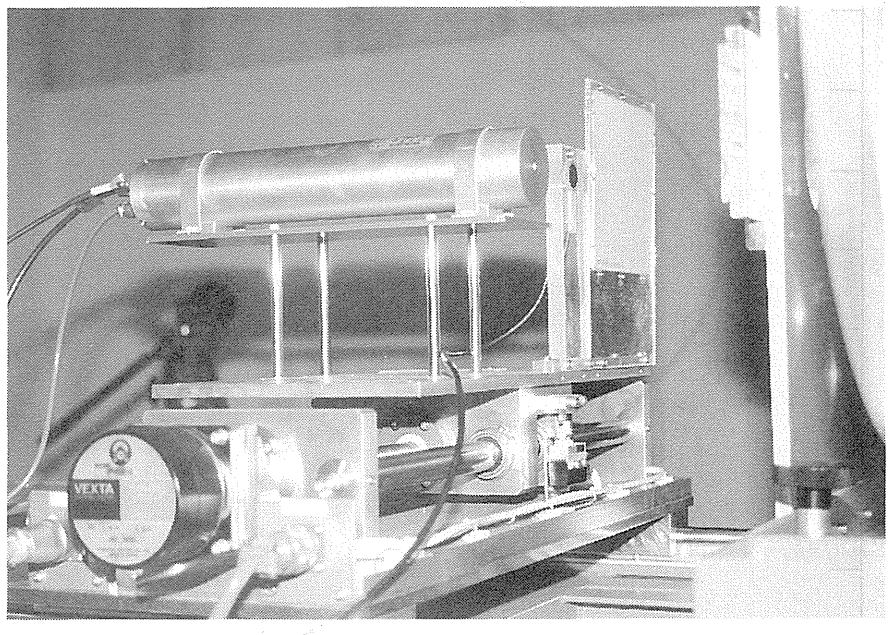

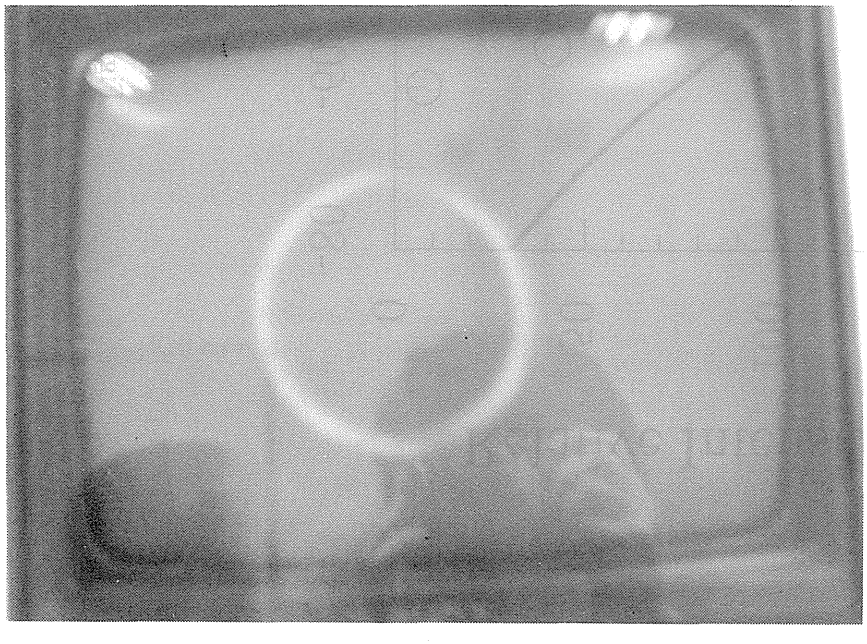

Fig. 3. Assembly of the zine phosphor screen, the small chamber and the scintillation counter(top, middle) Photograph of the circulating trace of the wobbled beam gleaming on the zine phosphor screen. (bottom)

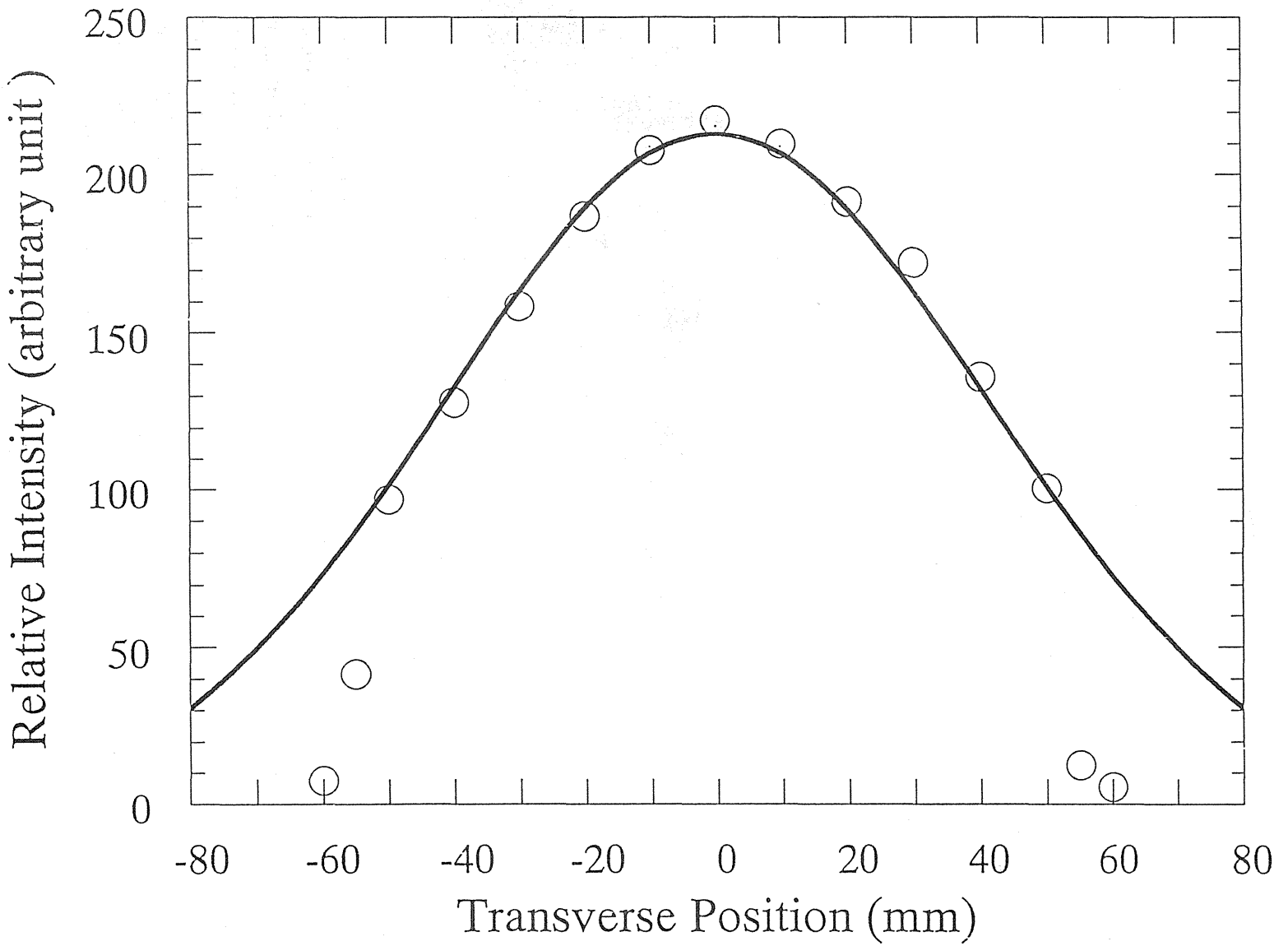


Fig. 4. Intensity distribution of 135 MeV/u carbon beam at the irradiation site by the gold scatterer of 0.27 mm thickness.

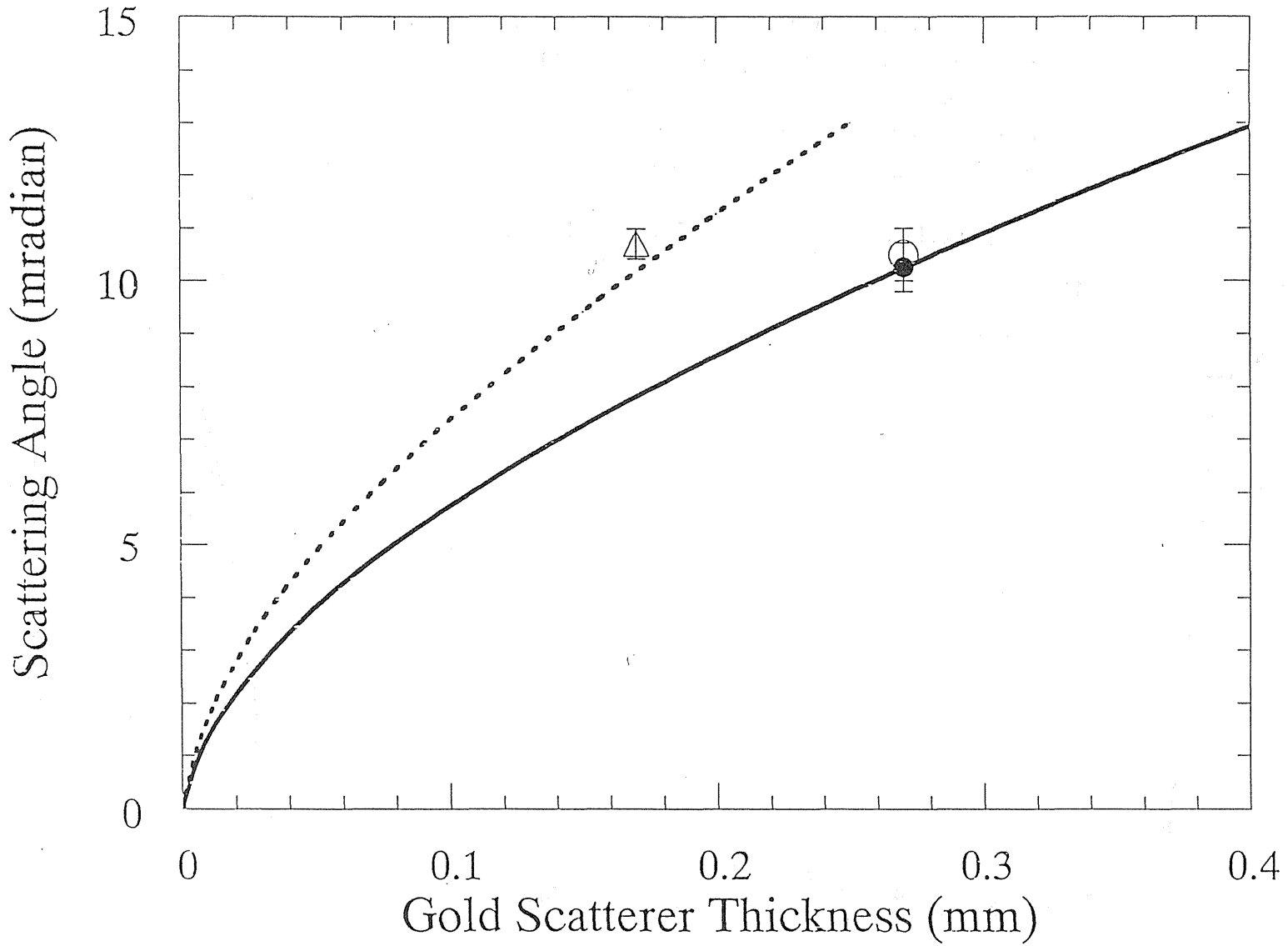


Fig. 5. Root mean square of the scattered angles for 95 MeV/u Ar(open triangle), 135 MeV/u carbon(open circle), and 135 MeV/u neon (closed circle) beams.

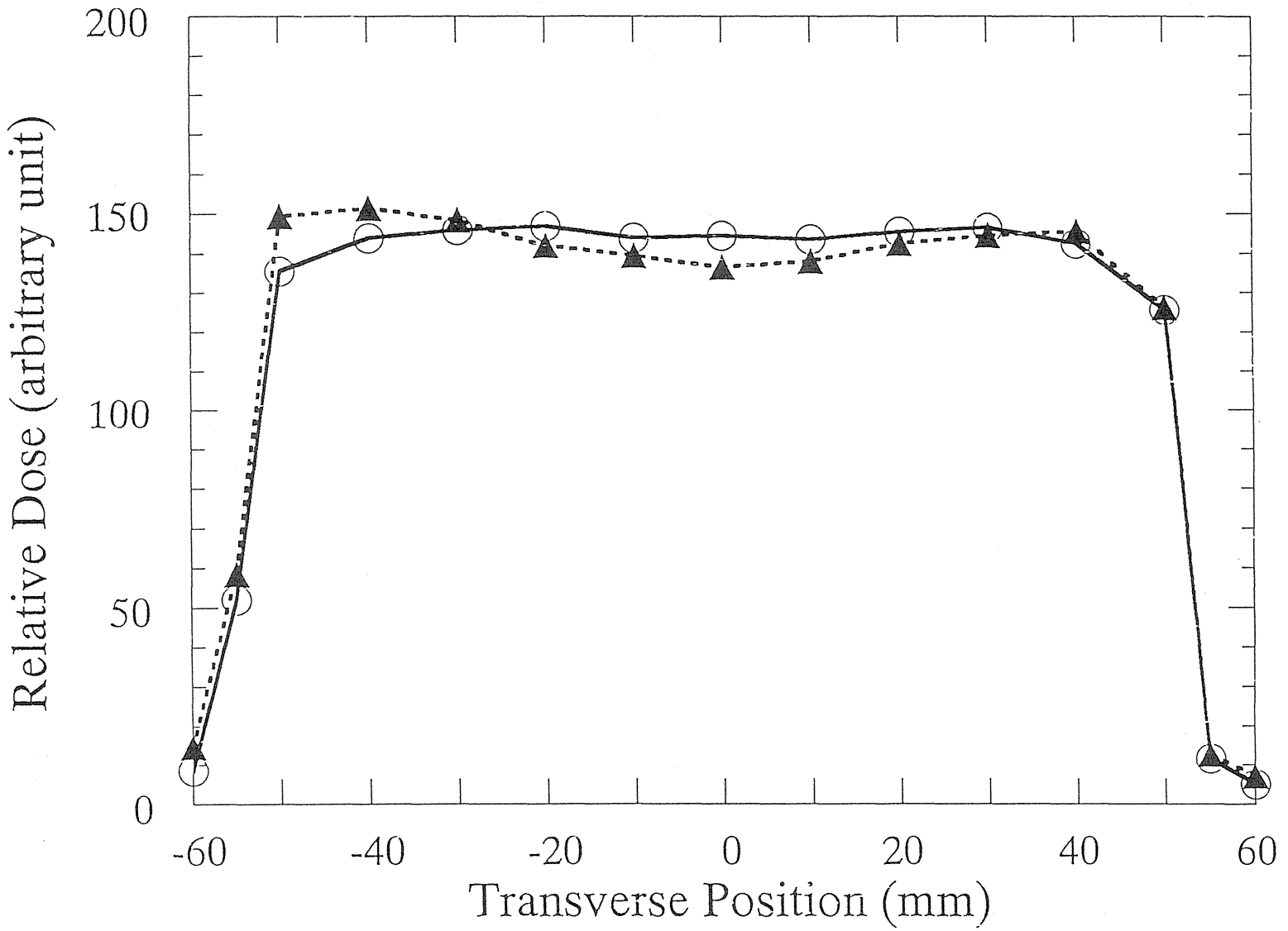


Fig. 6. Intensity distribution of irradiation fields of carbon beam at the irradiation site. Open circles and closed triangles show the distributions realized by circulating the scattered beam with a radius of 56.7 mm and 60.0 mm, respectively.

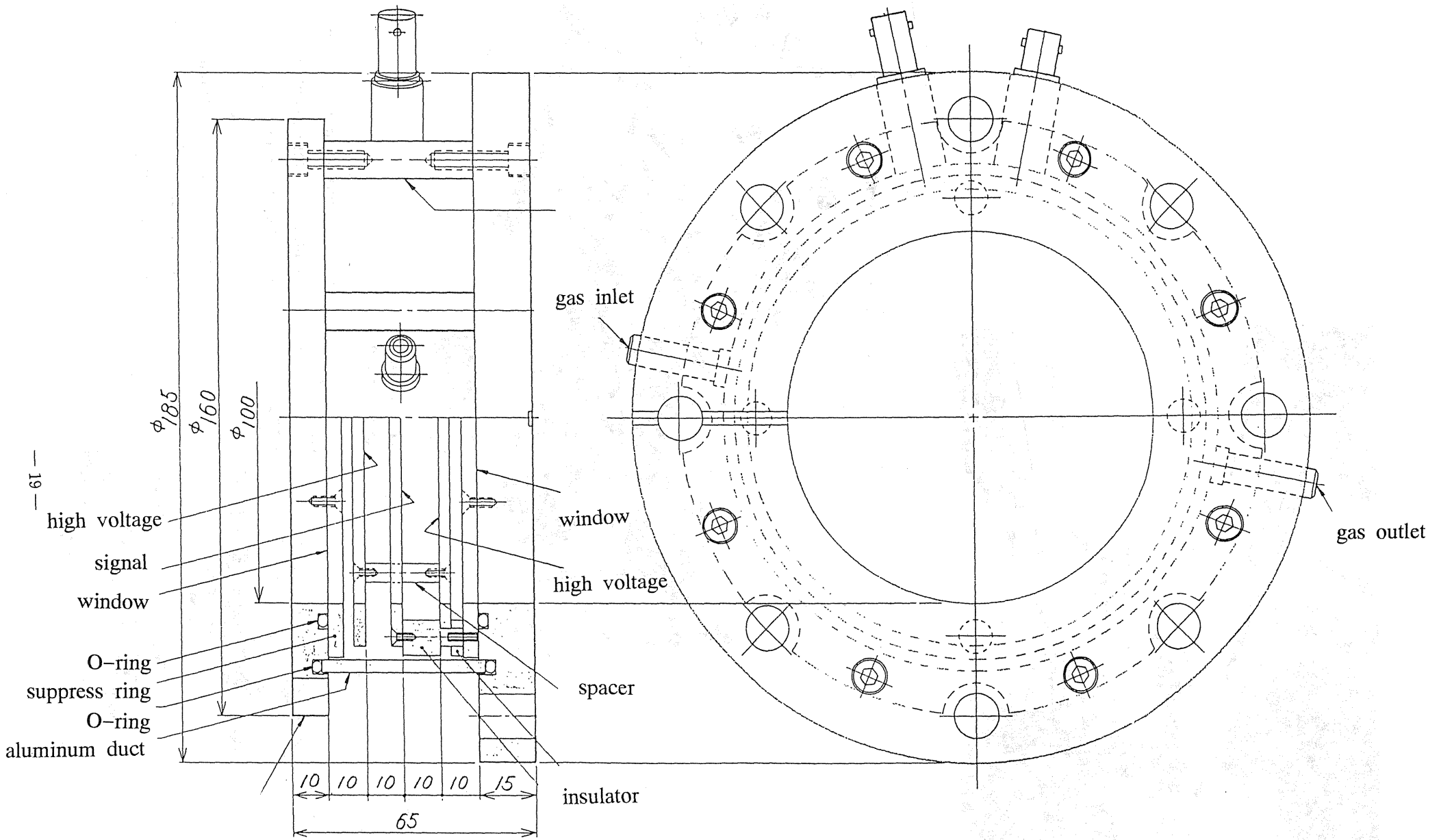


Fig. 7. Illustration of the irradiation monitor chamber.

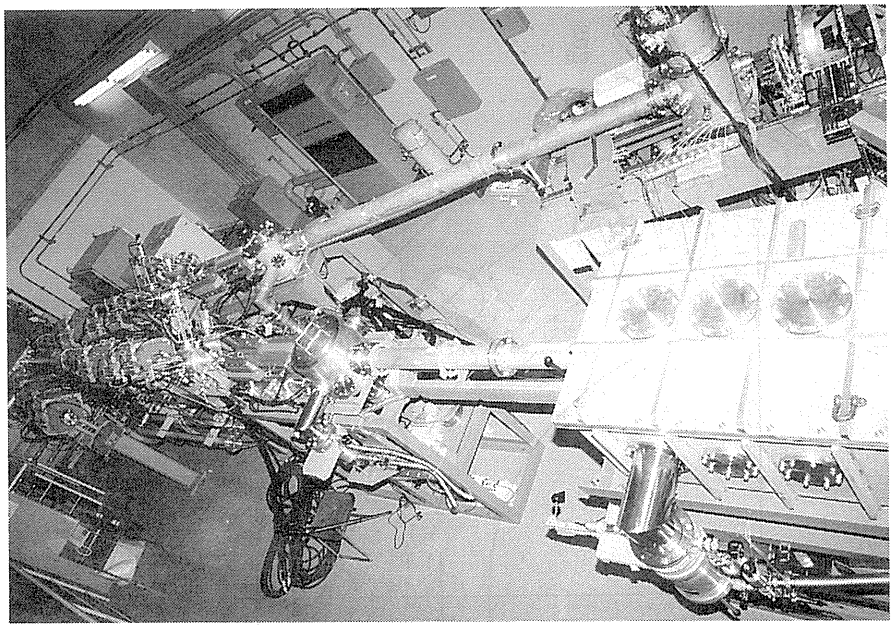

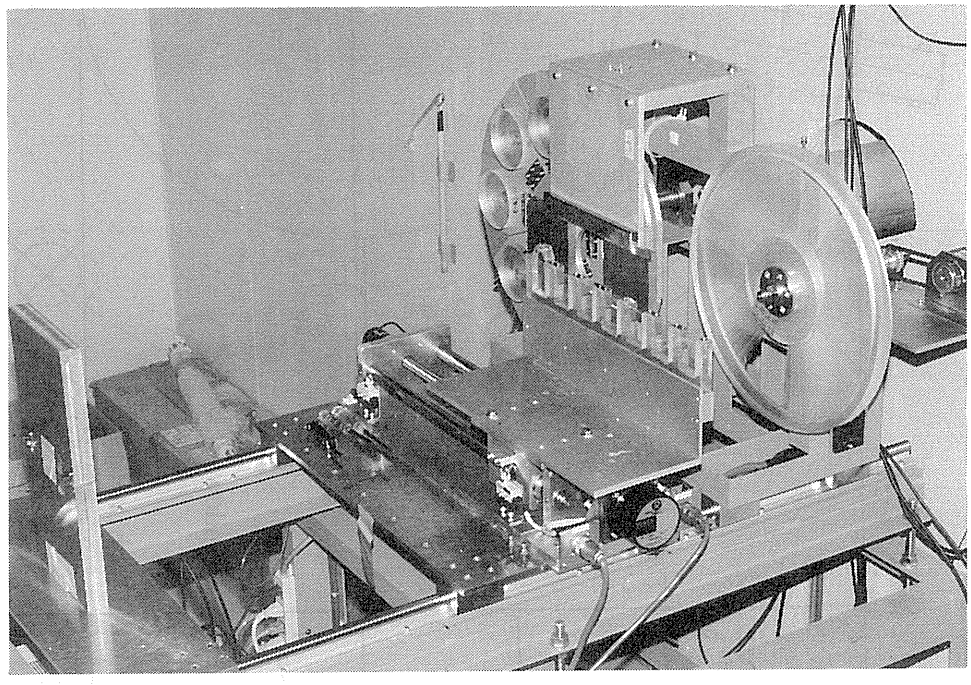

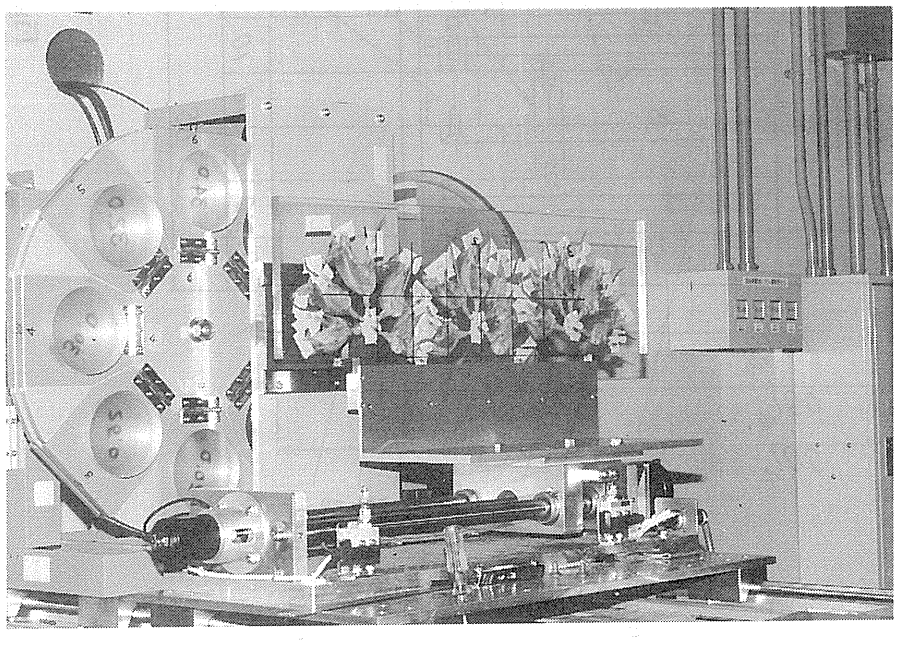

Fig. 8. Photographs of the irradiation system installed at the RIKEN ring cyclotron facility. The upper stream (top), around the irradiation site (middle and bottom) of the irradiation port.

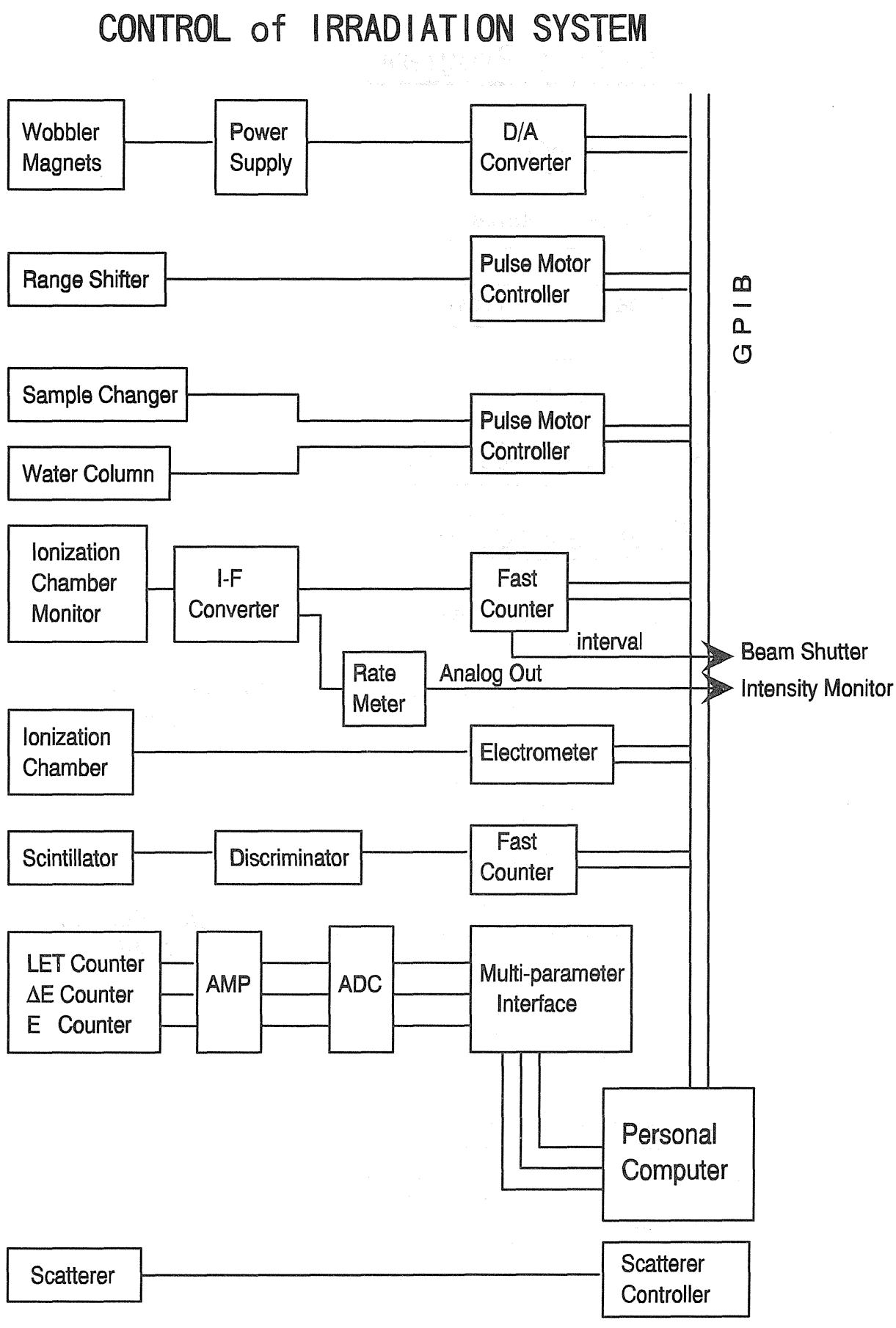


Fig. 9. Block diagram of the control system.

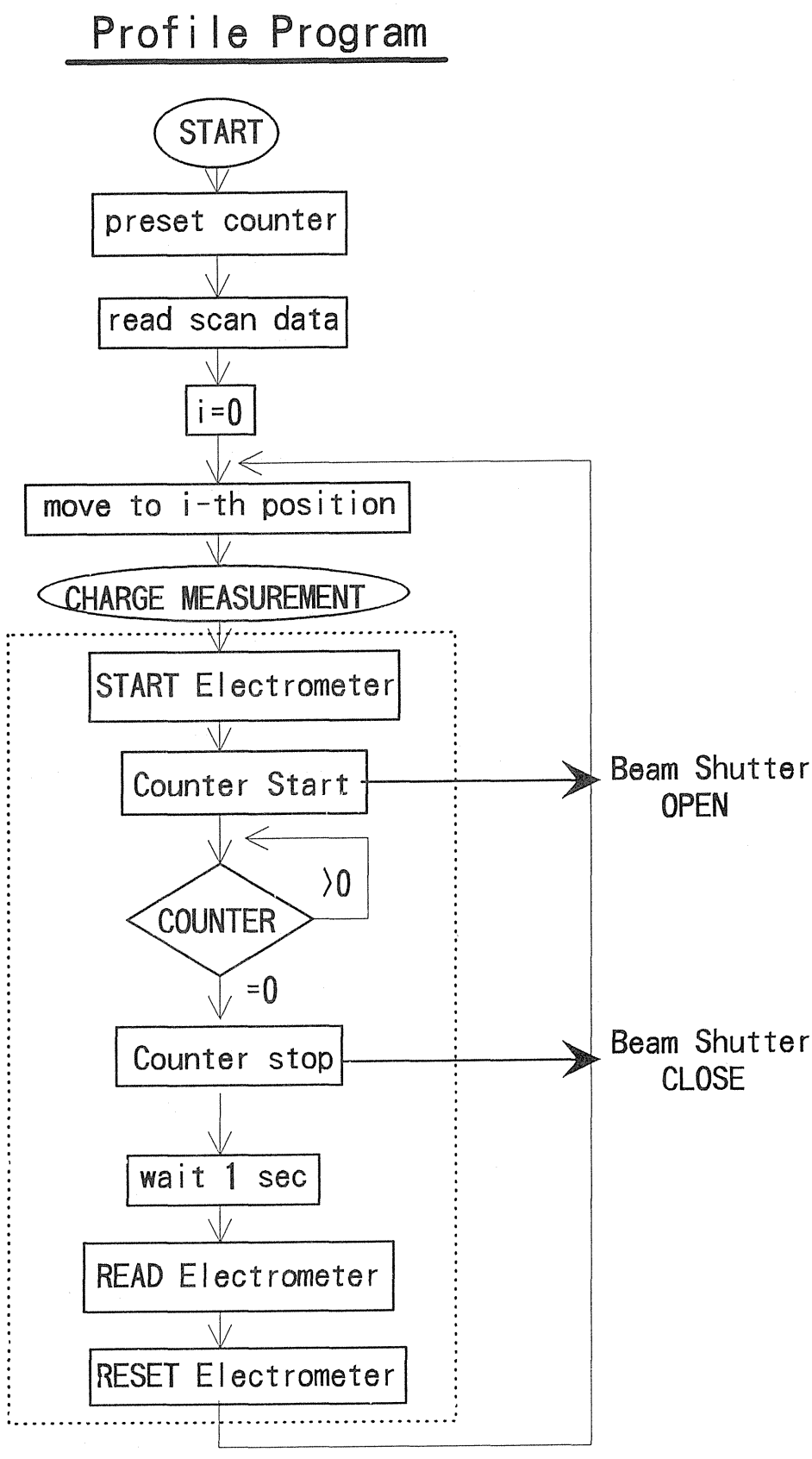


Fig. 10. Flow chart of the program "PROFILE".

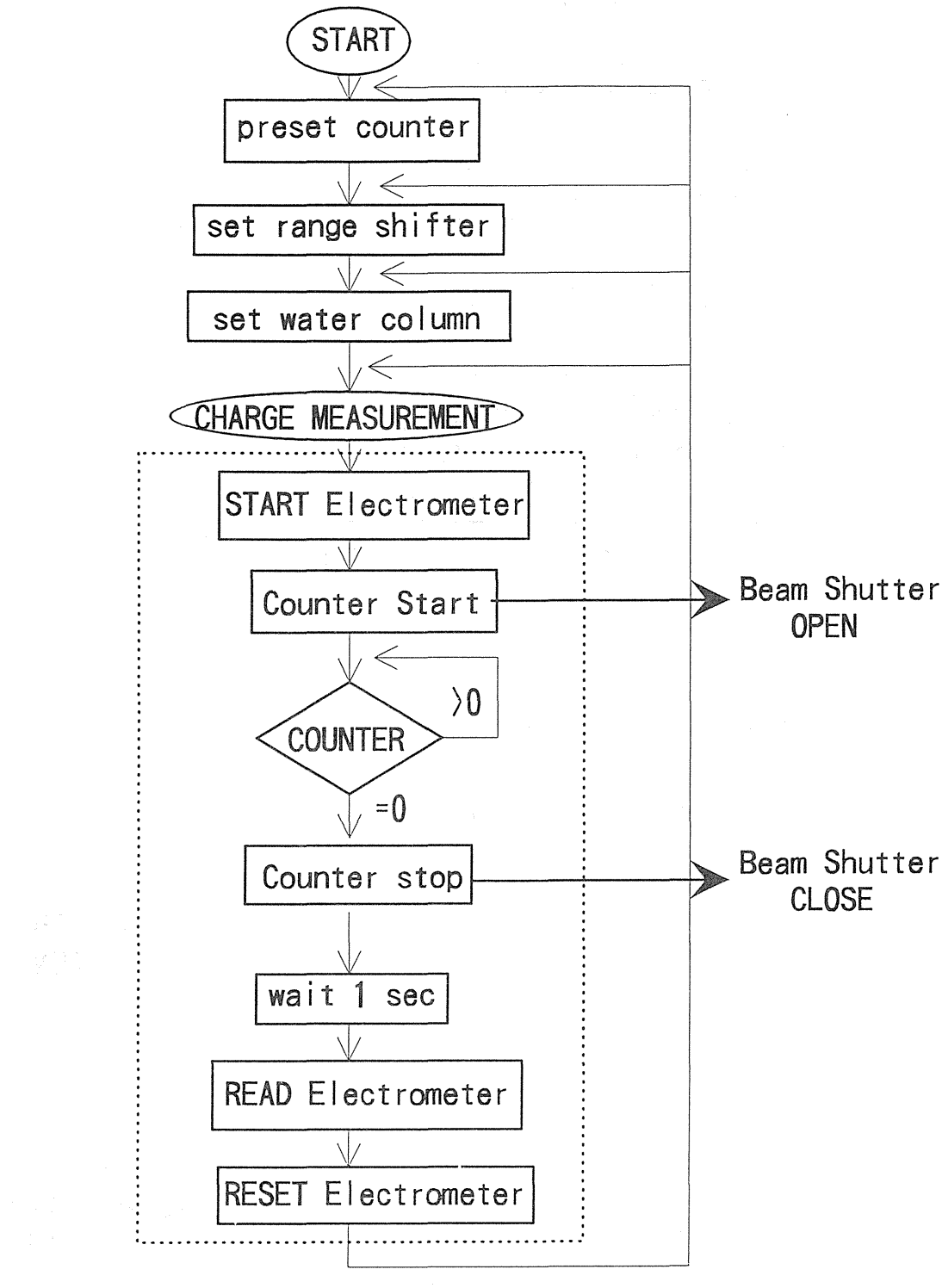


Fig. 11. Flow chart of the program "BRAGG".

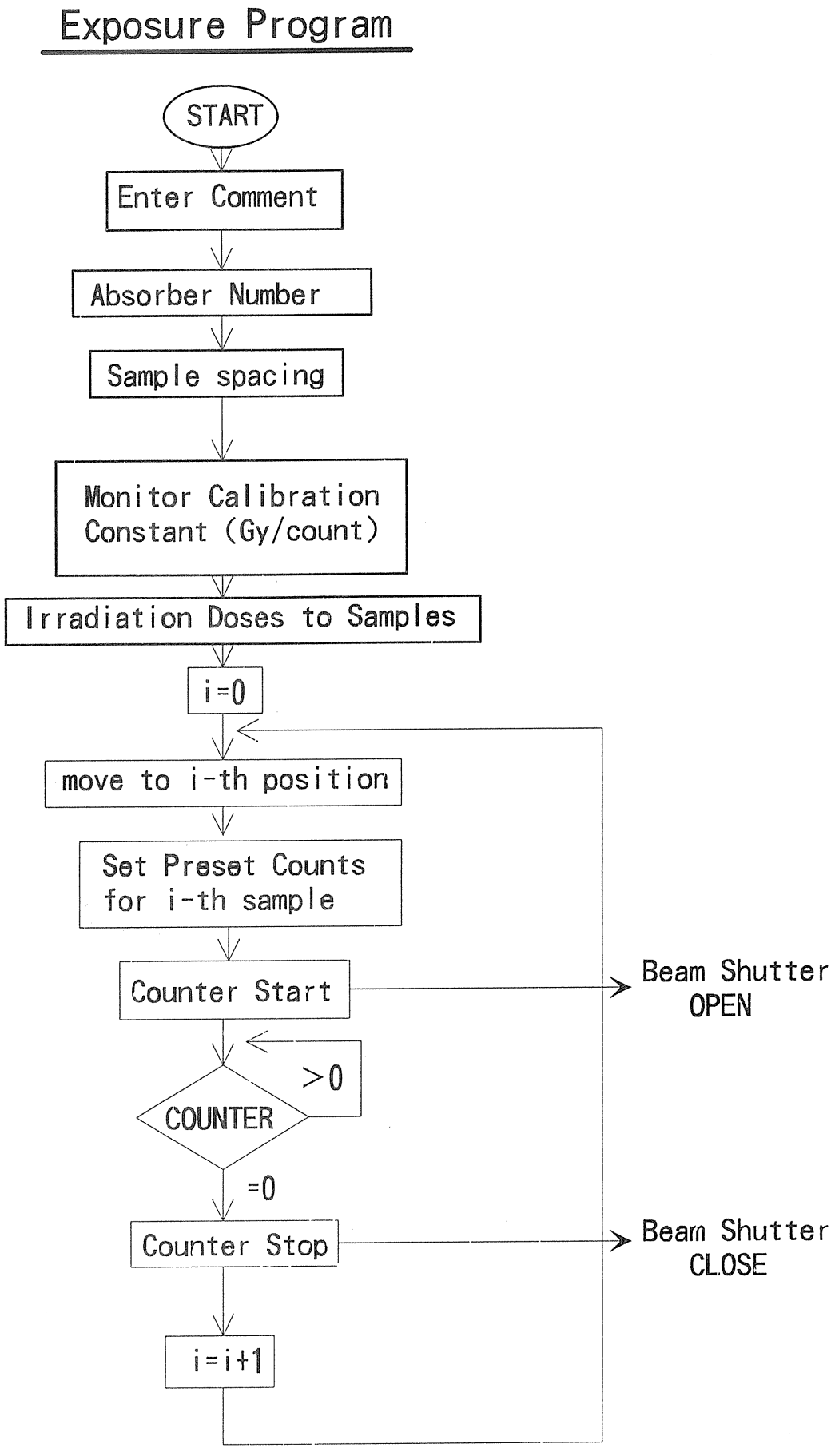


Fig. 12. Flow chart of the program "EXPOSURE".

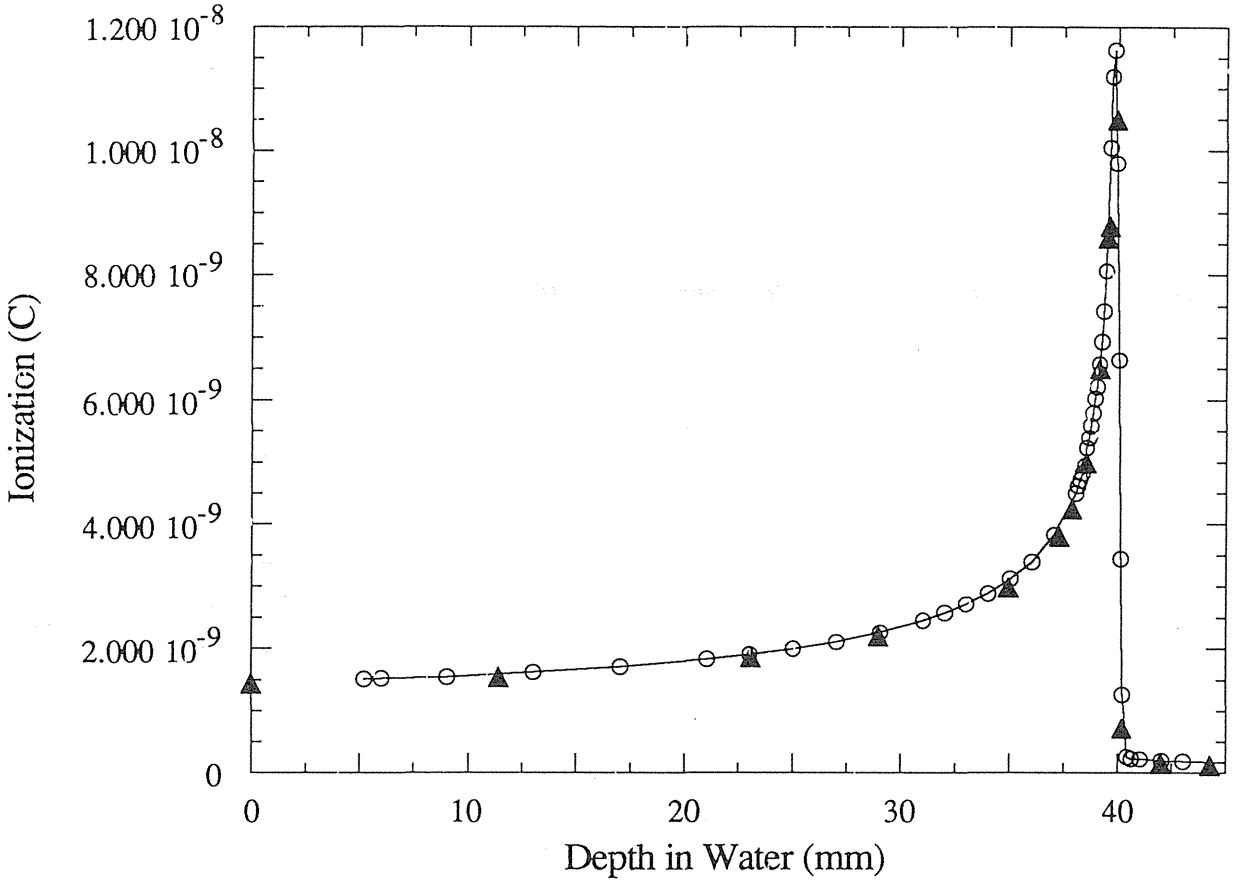


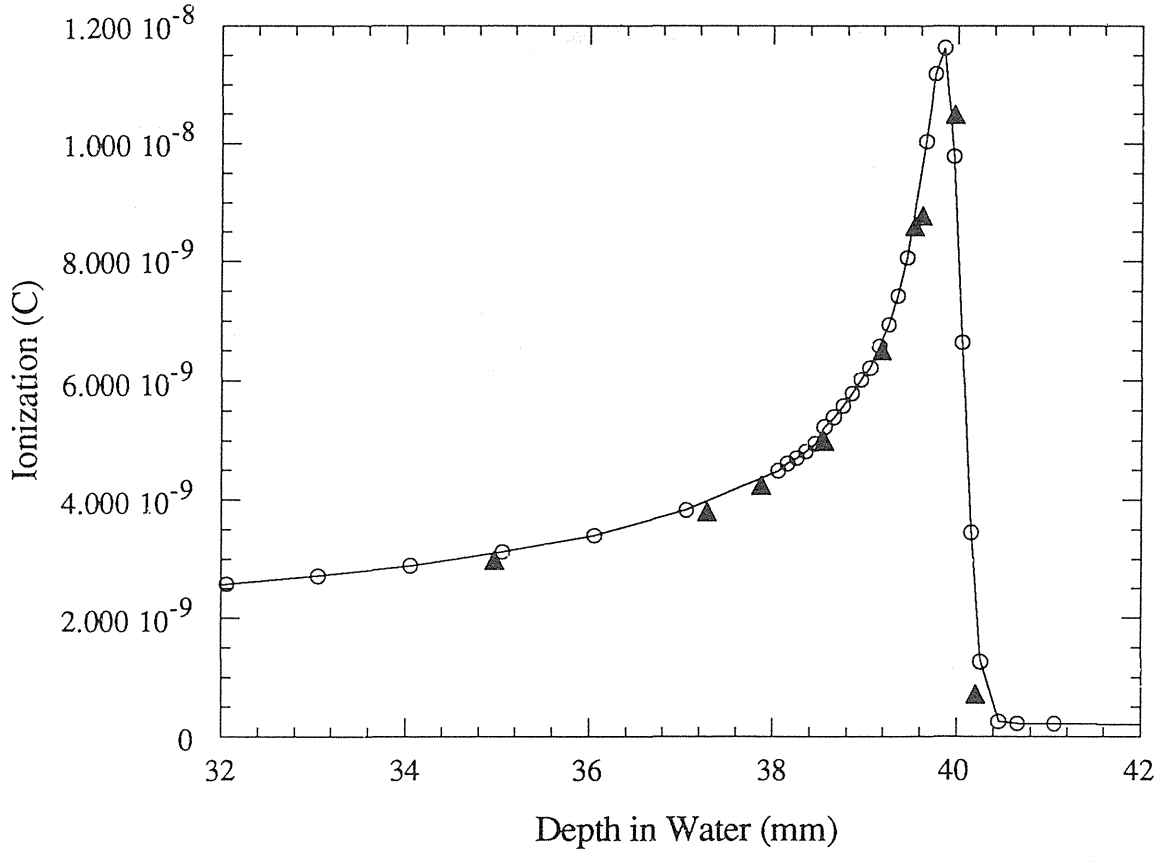


Fig. 13. Comparison of the Bragg curves measured with the range shifter(closed triangles) and water column (open circles), which is horizontally shifted 5.059 mm. The expanded graph near the Bragg peak is shown in a lower graph.

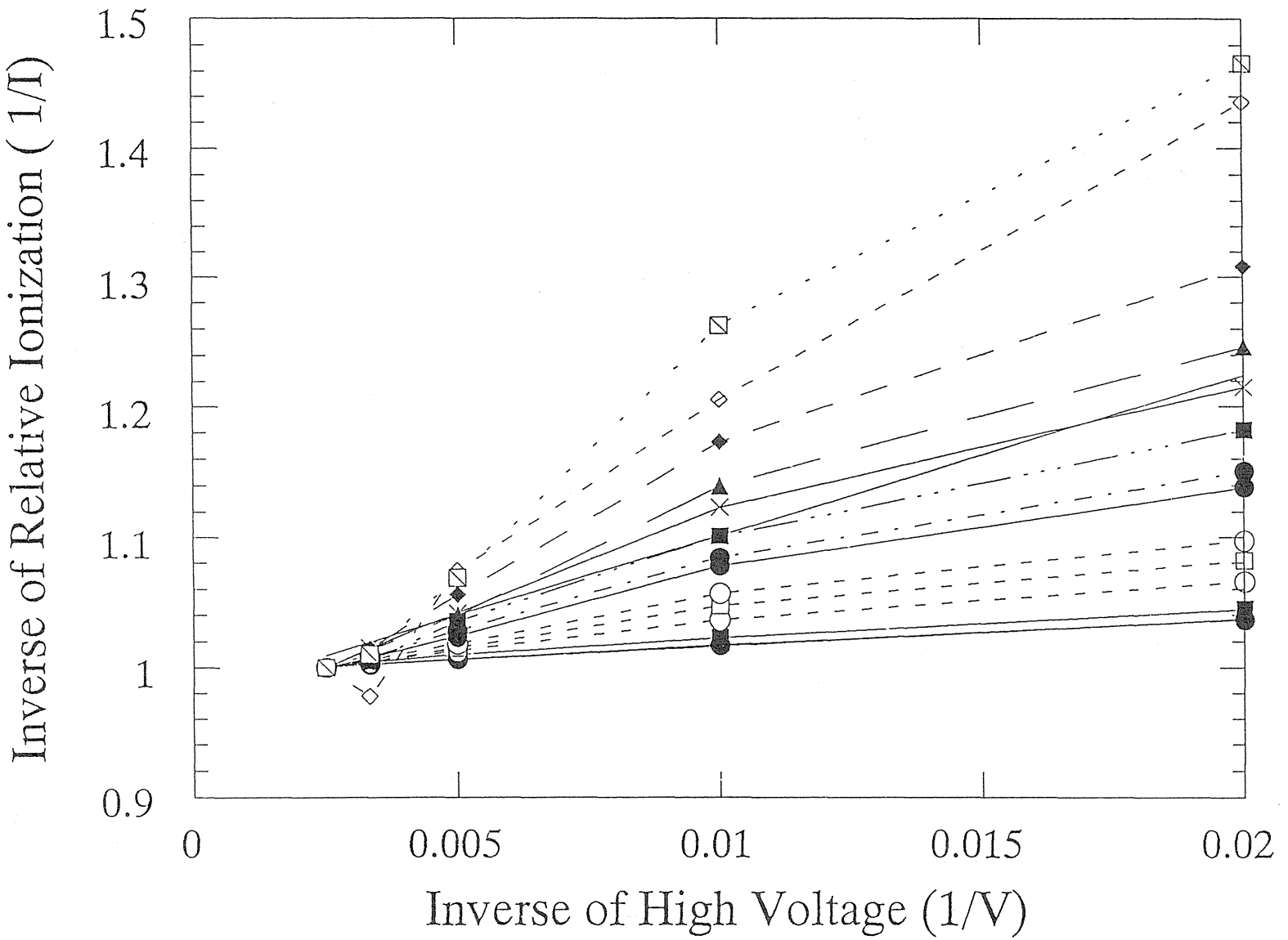


Fig. 14. Inverse of the ionization current versus inverse of the applied high voltage.

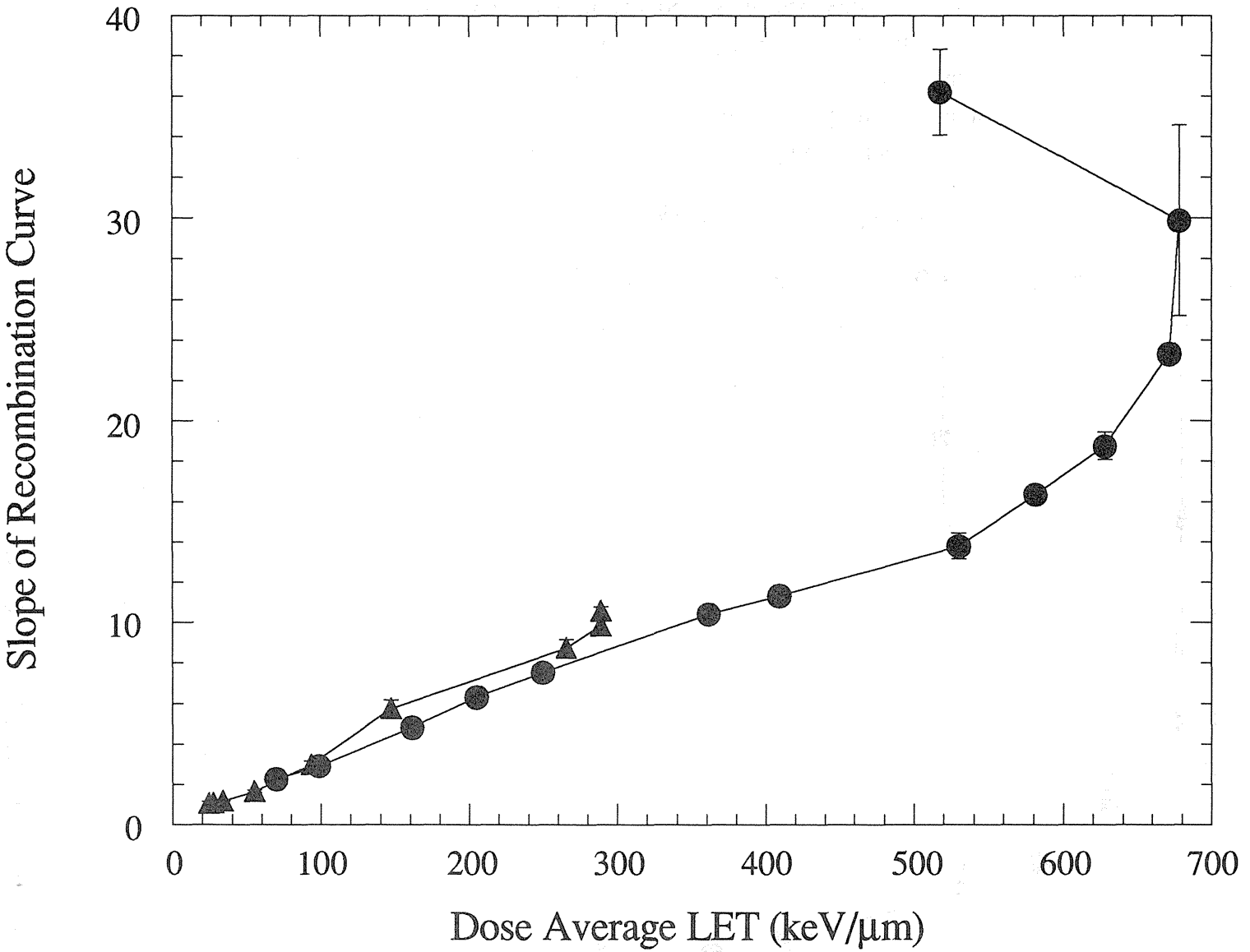


Fig. 15. LET dependence of the slopes of the initial recombination curves. Closed circles and triangles show the slopes for the case of neon and carbon beams, respectively.

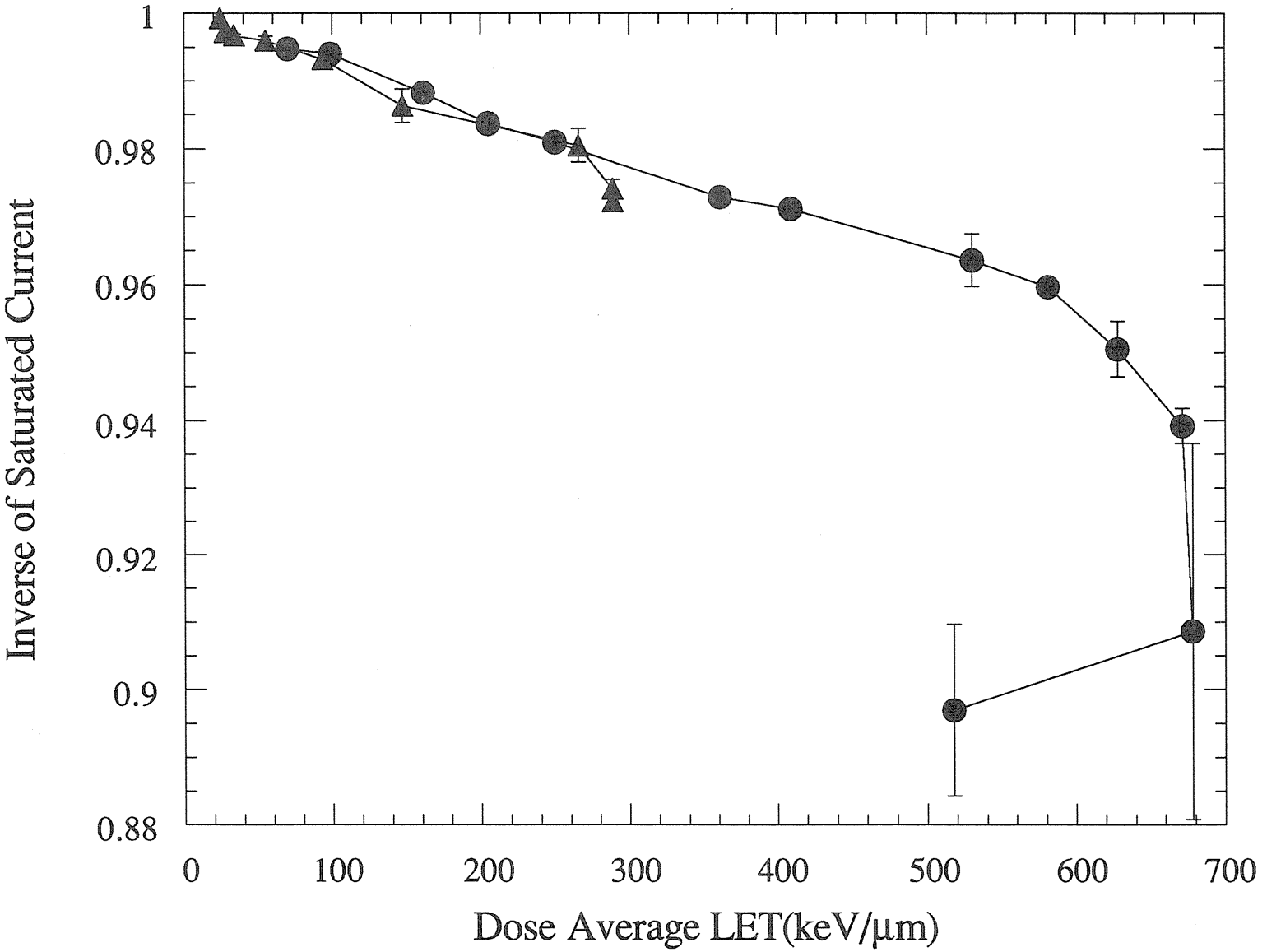


Fig. 16. LET dependence of the extrapolated values of the inverse of the ionization current at infinitely high voltage of the chamber. Closed circles and triangles show the extrapolated values for the case of neon and carbon beams, respectively.

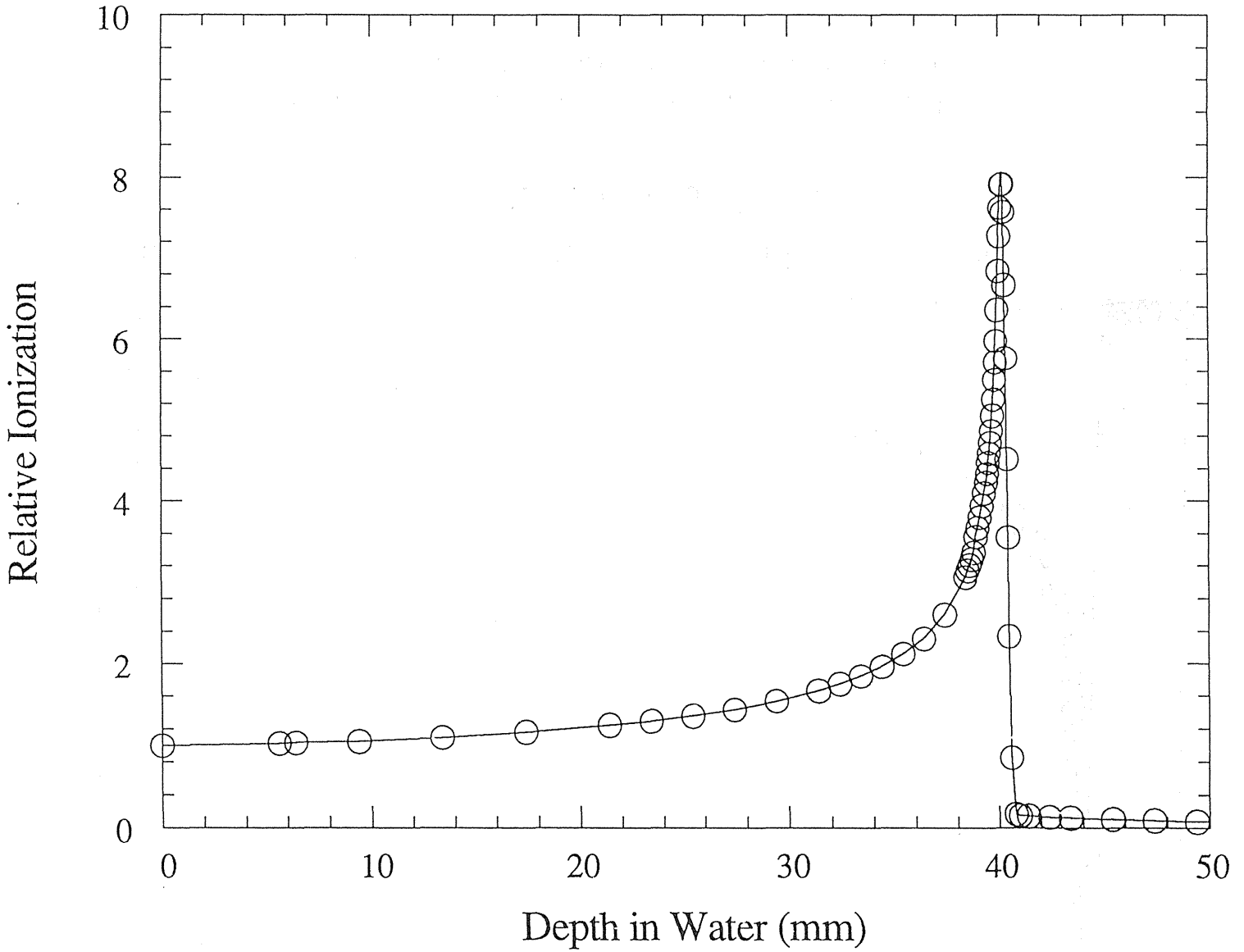


Fig. 17. Comparison of the two Bragg curves, a raw ionization curve(open circles) and a Bragg curve corrected by the initial recombination effect (solid curve) in case of carbon beam.

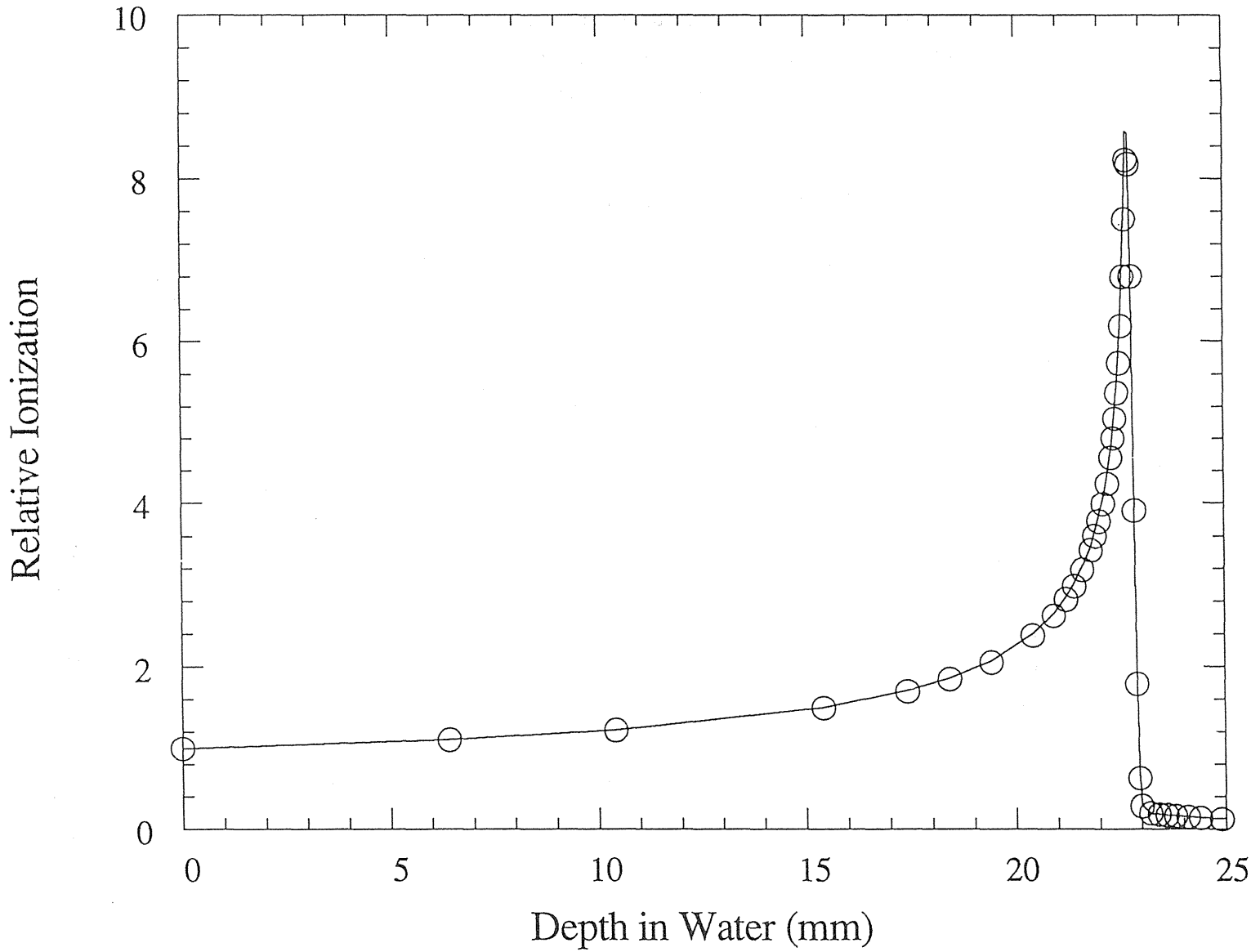


Fig. 18. Comparison of a raw ionization curve and the corrected Bragg curve in case of neon beam.

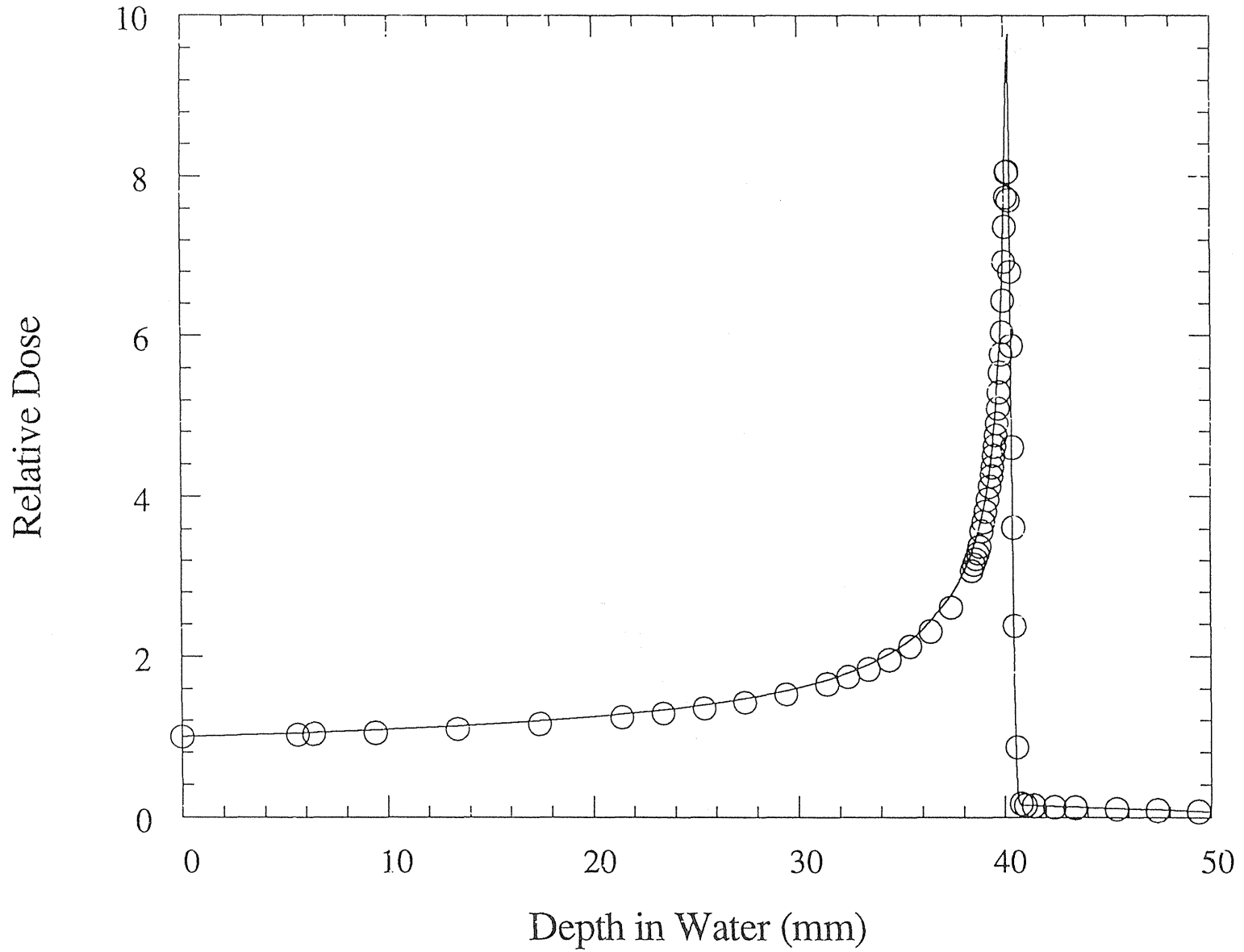


Fig. 19. Depth dose distribution in water for 135 MeV/u carbon beam. Open circles and the solid curve show the experimental and theoretical results, respectively.

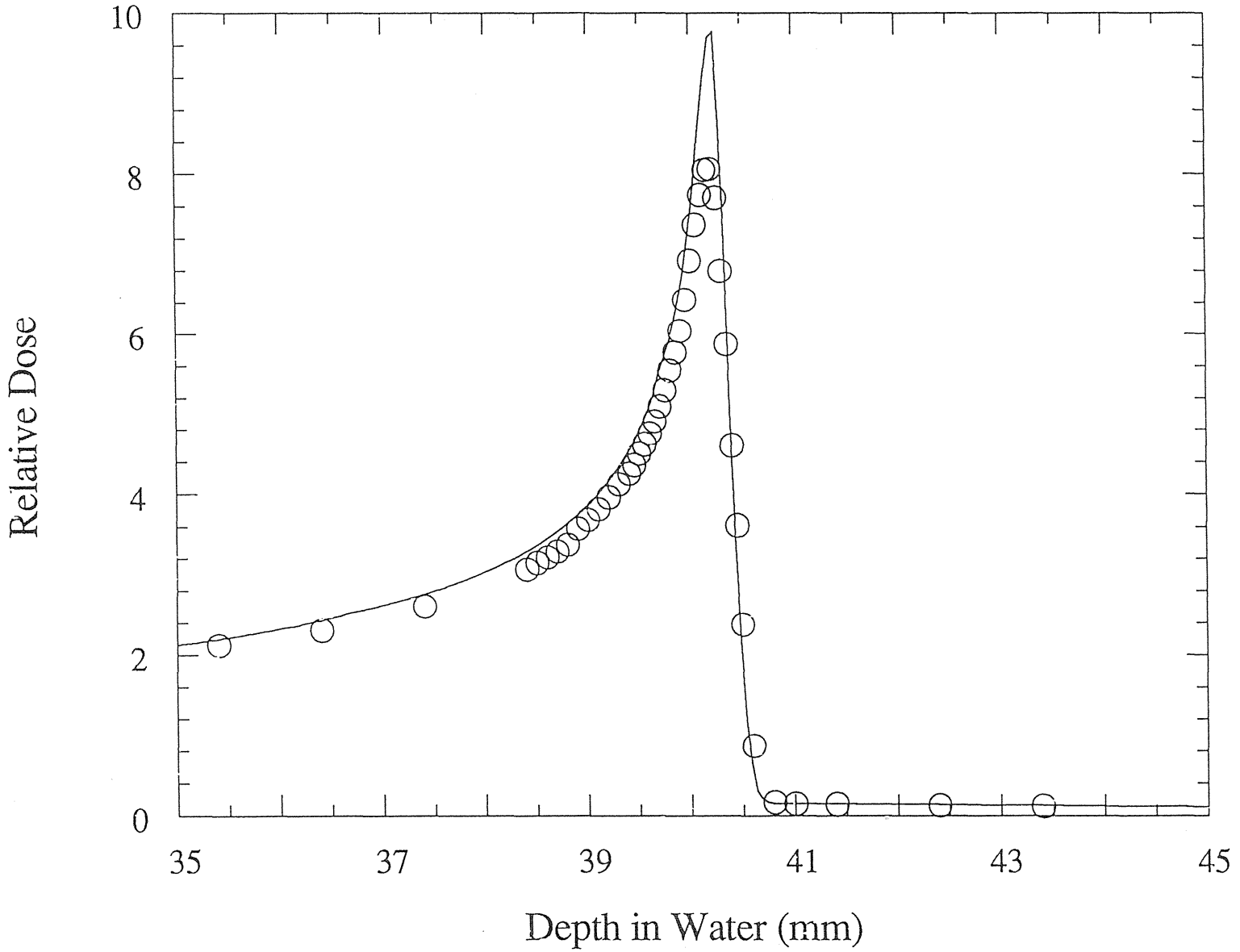


Fig. 20. Expanded depth dose distribution in water for 135 MeV/u carbon beam.

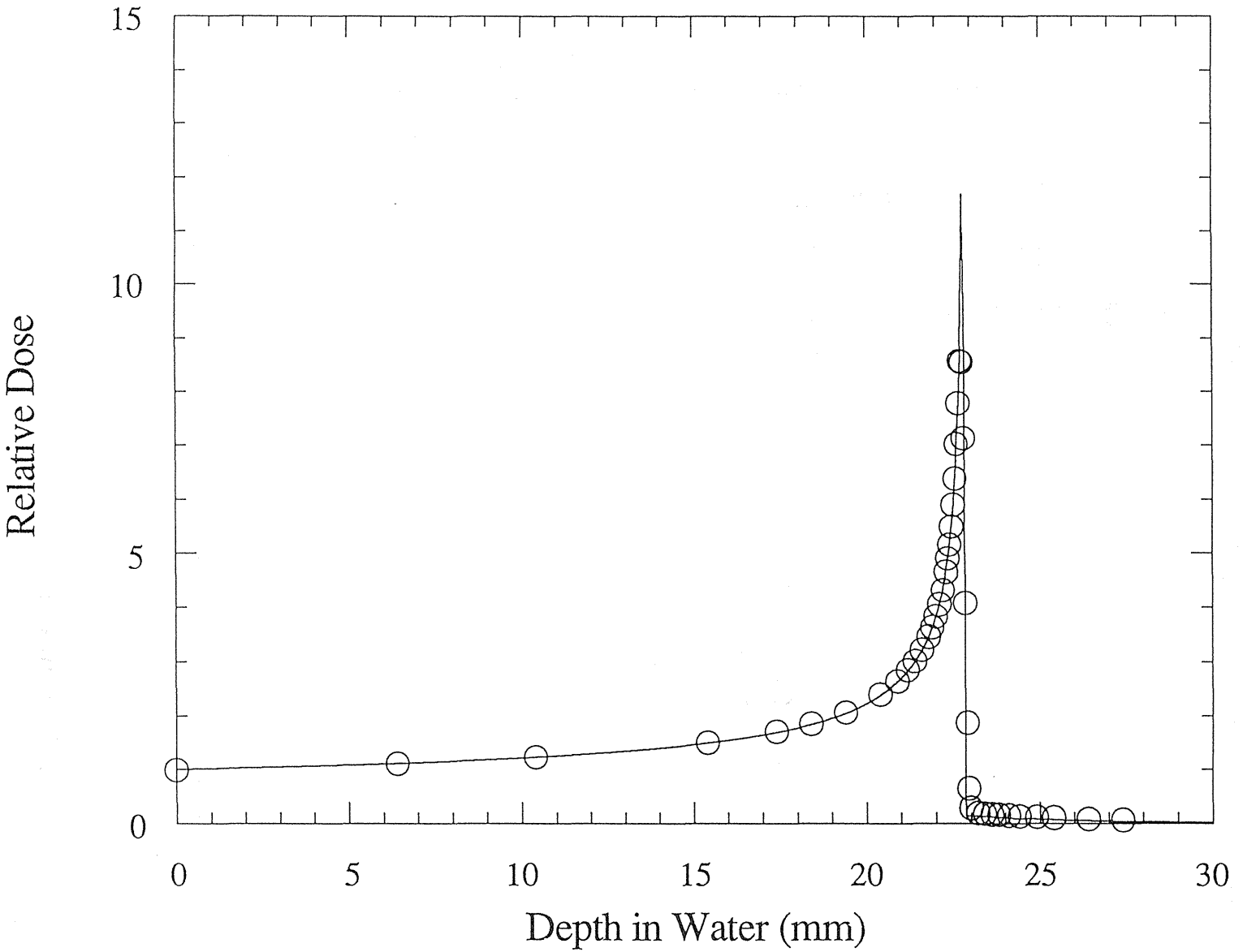


Fig. 21. Depth dose distribution in water for 135 MeV/u neon beam. Open circles and the solid curve show the experimental and theoretical results, respectively.

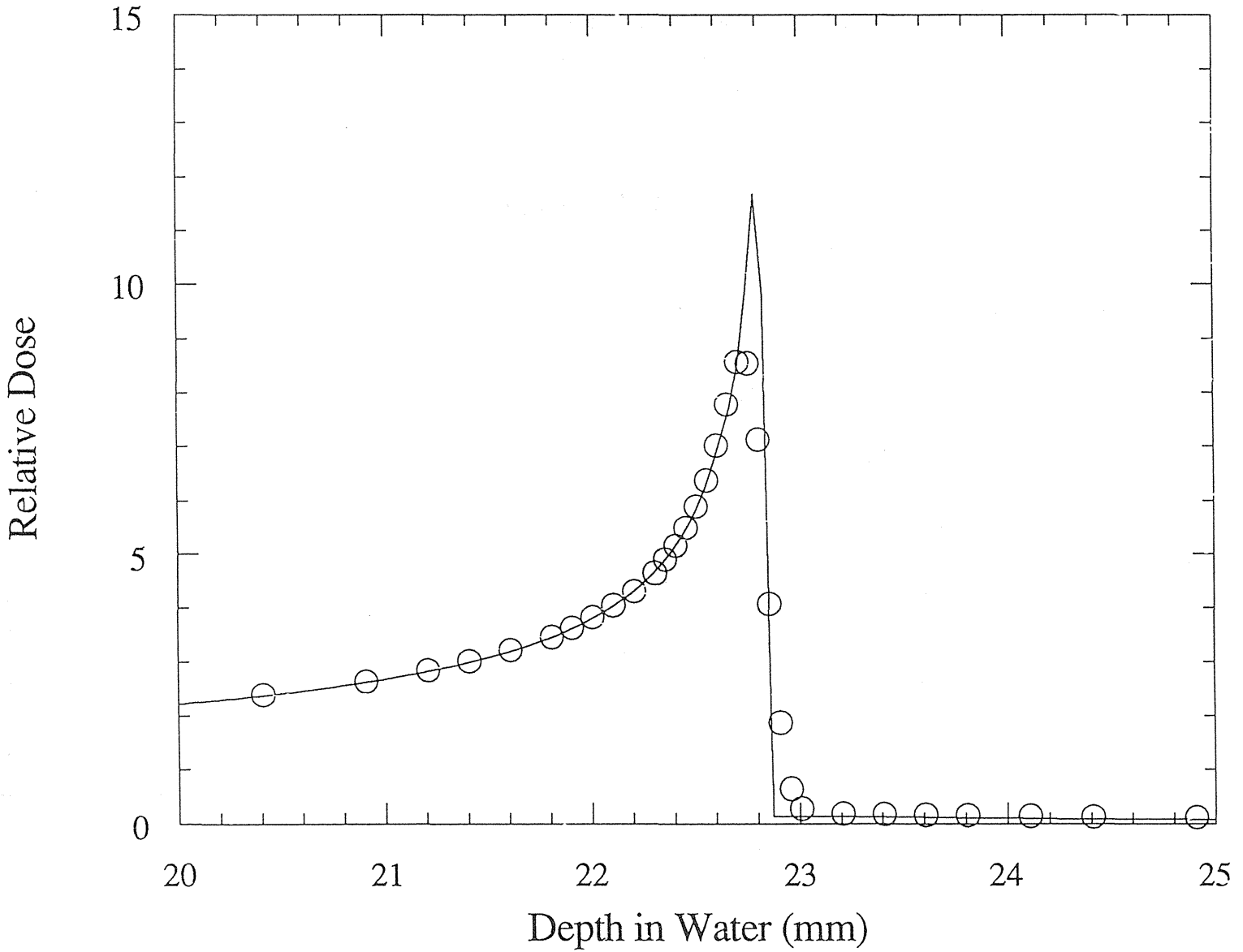


Fig. 22. Expanded depth dose distribution in water for 135 MeV/u neon beam.

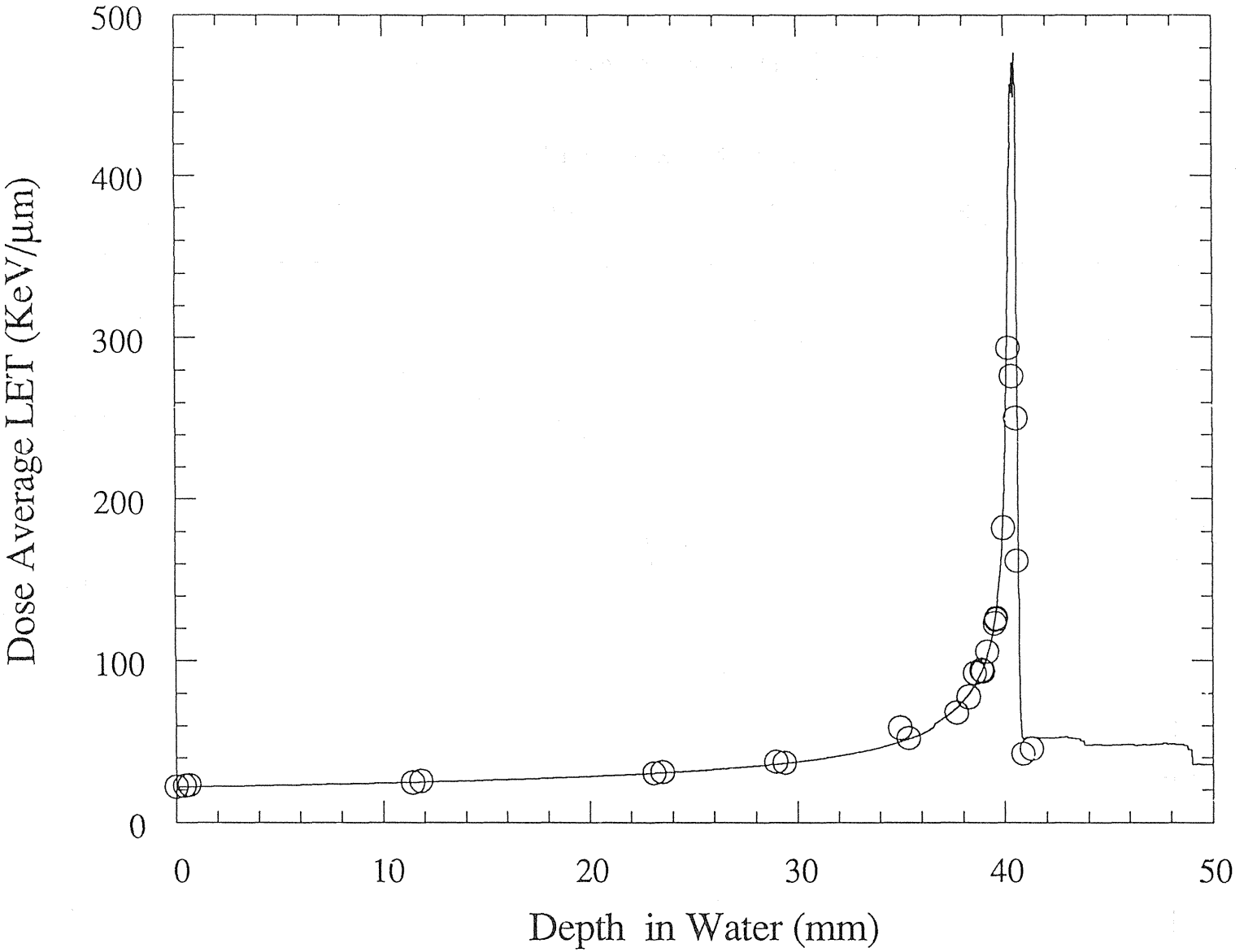


Fig. 23. Dose average LET for 135 MeV/u carbon beam in water. Open circles and solid curve show the experimental and theoretical results, respectively.

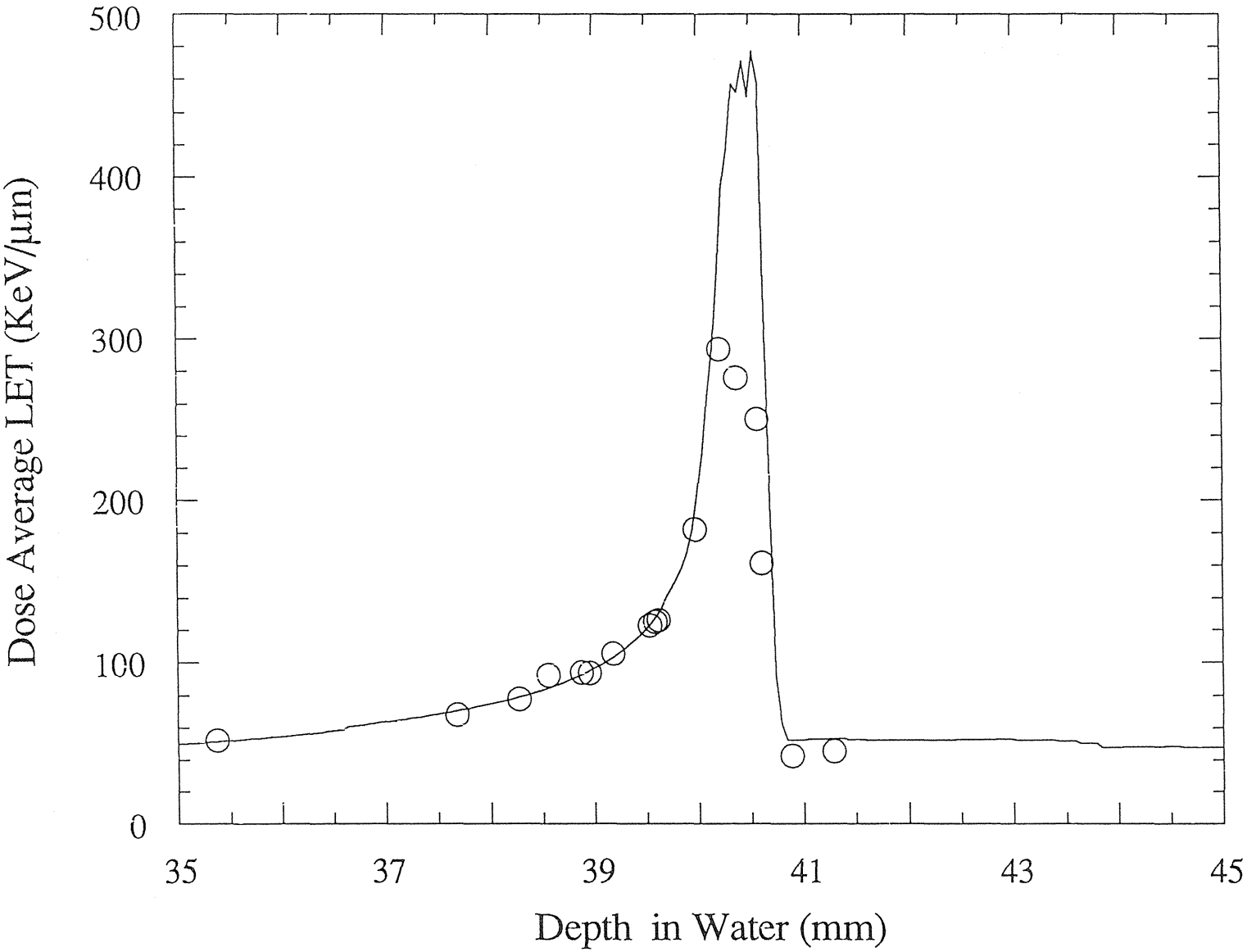


Fig. 24. Expanded graph of Fig. 23.

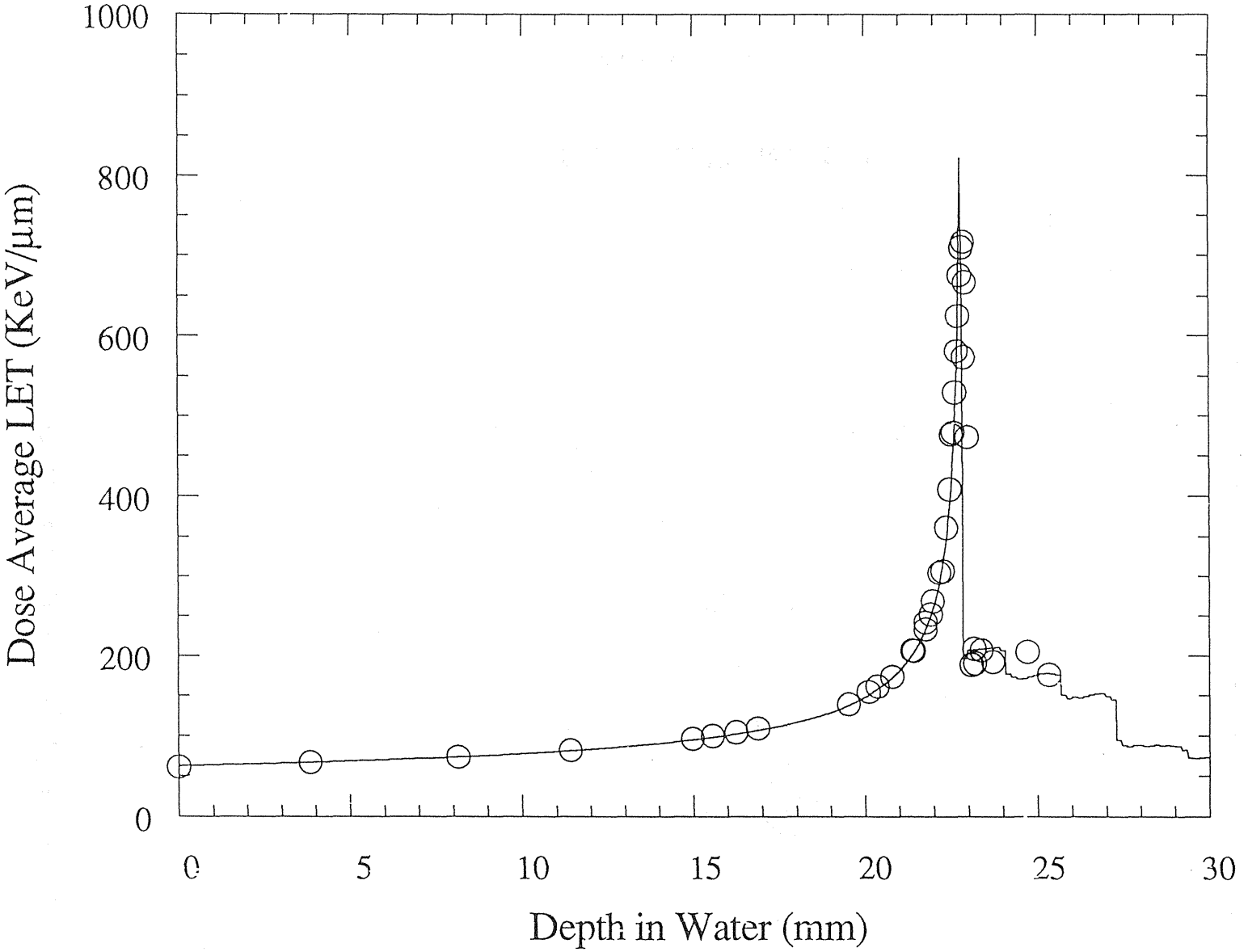


Fig. 25. Dose average LET for 135 MeV/u neon beam in water. Open circles and solid curve show the experimental and theoretical results, respectively.

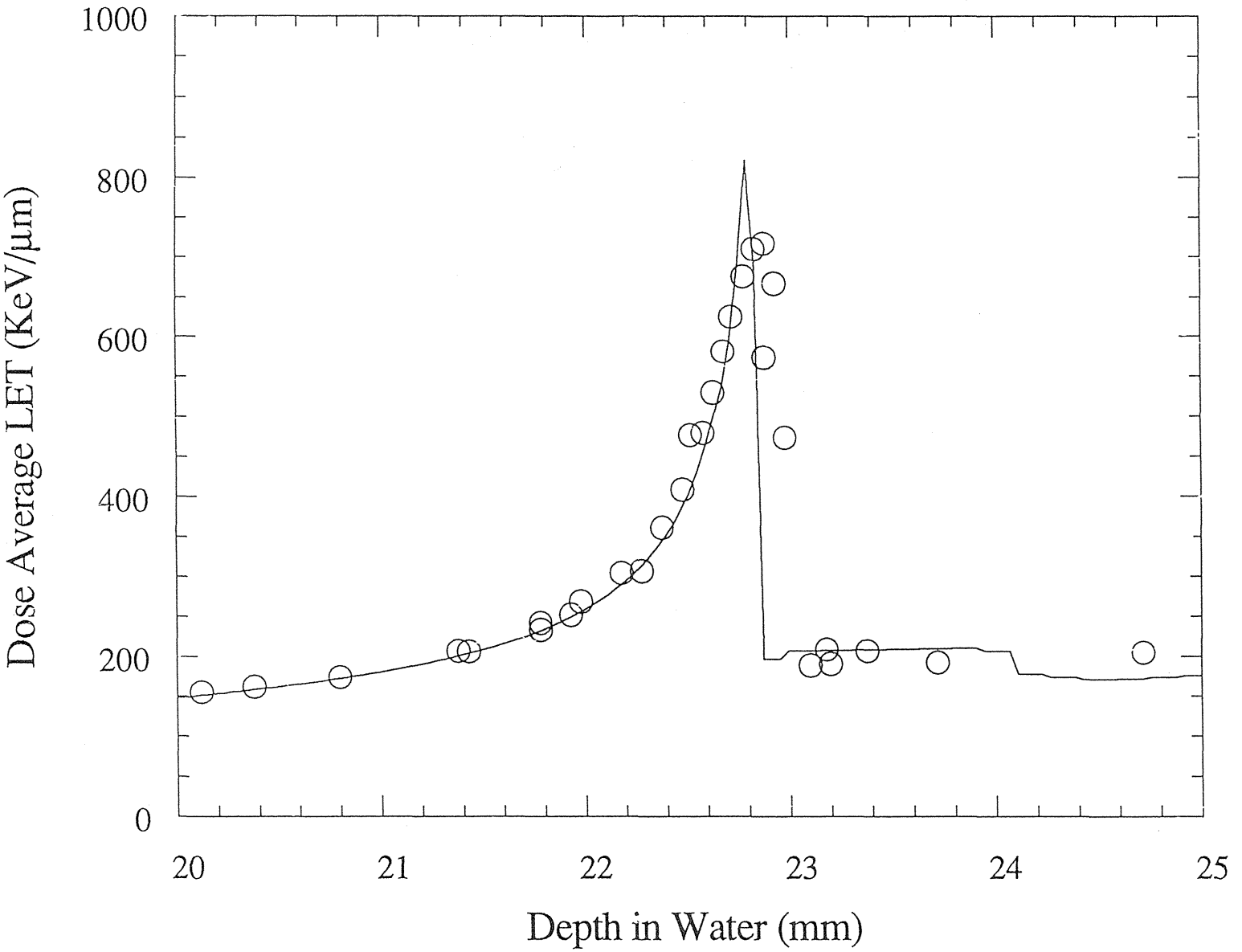


Fig. 26. Expanded graph of Fig. 25.

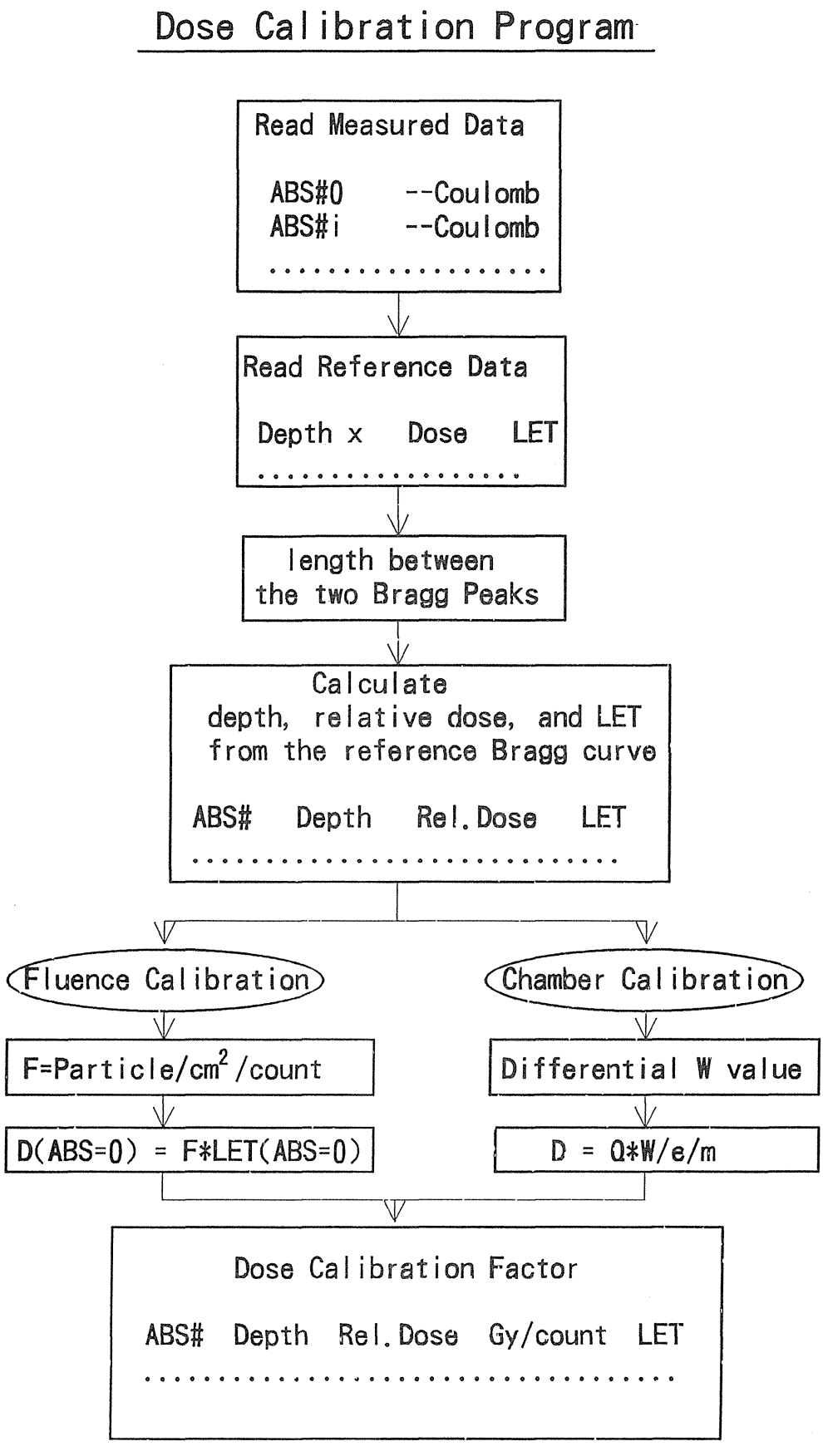


Fig. 27. Flow chart of the program "DCALIB" for the heavy-ion dosimetry.